CAMBRIDGE
UNIVERSITY PRESS

RESEARCH ARTICLE

Guaranteed real-time cooperative collision avoidance for *n*-DOF manipulators

Erick J. Rodríguez-Seda [ID] and Michael D. M. Kutzer [ID]

Deparment of Weapons, Robotics, and Control Engineering, United States Naval Academy, Annapolis, MD, USA
**Corresponding author:** Erick J. Rodríguez-Seda; Email: rodrigue@usna.edu

Abstract

This paper presents a decentralized, cooperative, real-time avoidance control strategy for robotic manipulators. The proposed avoidance control law builds on the concepts of artificial potential field functions and provides tighter bounds on the minimum safe distance when compared to traditional potential-based controllers. Moreover, the proposed avoidance control law is given in analytical, continuous closed form, avoiding the use of optimization techniques and discrete algorithms, and is rigorously proven to guarantee collision avoidance at all times. Examples of planar and 3D manipulators with cylindrical links under the proposed avoidance control are given and compared with the traditional approach of modeling links and obstacles with multiple spheres. The results show that the proposed avoidance control law can achieve, in general, faster convergence, smaller tracking errors, and lower control torques than the traditional approach. Furthermore, we provide extensions of the avoidance control to robotic manipulators with bounded control torques.

1. Introduction

Robotic manipulators are used in a wide range of applications, including handling of hazardous materials, sorting facilities, manufacturing and assembling lines, construction, and health care, to name a few [1]. In all these scenarios, the manipulators are expected to interact with their environment, which may involve the presence of obstacles, people, and other robots. For instance, consider the two 3-degrees-of-freedom (DOF) articulated robots in Fig. 1. The robots need to avoid collisions not only with static and dynamic objects in their environment but also with other robots and with themselves. Therefore, it is critical to develop control protocols that can guarantee the safety of the manipulators at all times.

1.1. Related work

Collision avoidance for robotic manipulators can be solved using motion planning algorithms, where the objective is to design a safe trajectory for the manipulator to follow over some period of time, or real-time control, where control inputs are updated online based on the continuous interaction and perception of the robot with its surrounding. Several motion planning algorithms have been proposed over the years [2]. Examples include the use of C-space obstacle [3], rapidly exploring random trees [4–6], probabilistic roadmaps [7], and model predictive control [8, 9]. Other frameworks incorporate the use of artificial potential field functions to compute a safe path [10, 11], define geometric algorithms to detect potential collisions [12–16], or use machine learning (ML) tools to learn obstacle avoidance strategies [17, 18]. Nevertheless, many of these methods assume global knowledge of the environment (i.e., a centralized approach which might be impractical) are not rigorously developed to guarantee collision avoidance at all times or may be based on kinematic models [19] that ignore dynamic properties of the manipulators
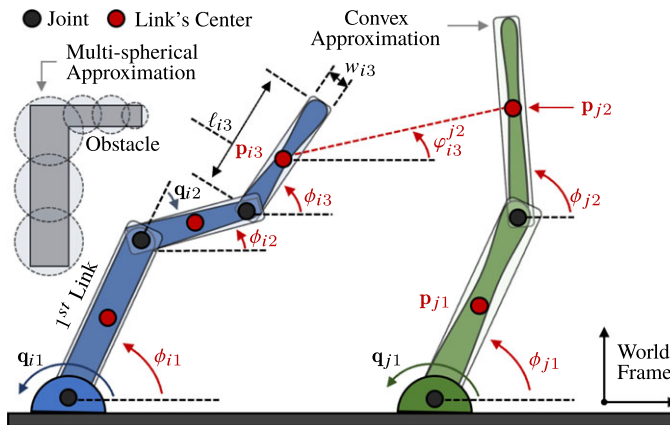
Figure 1. *Illustration of two robotic manipulators with an obstacle. Two different shape approximations or envelopes conventionally used in collision avoidance are represented: the use of a single convex shape on the manipulators and the use of multiple spheres on the obstacle.*

such as inertia, leading to non-smooth trajectories and potential collisions when maneuvering at high speeds. Furthermore, several applications, such as teleoperation, may involve robots that are not fully autonomous, for which the amount of planning might be constrained and where a real-time approach might be more suitable.

Real-time avoidance control, also known as reactive avoidance control, generates forces or control inputs that respond to information gathered at the moment either via sensing or communication. Of particular interest are distributed real-time avoidance frameworks that are provably safe, that is, that are theoretically guaranteed to avoid collisions at all times. For instance, frameworks based on artificial potential fields [20, 21] can be implemented in a decentralized manner and can be rigorously proven to avoid collision by applying Lyapunov theory. Examples include the works in [22–27]. A common drawback of these approaches is the modeling of links and segments of obstacles as spheres, a collection of spheres [26, 28] (see Fig. 1 for the obstacle in the example), or other primitive shapes [11, 29, 30] which may lead to the implementation of several artificial potential field functions or unnecessary conservatism due to the loose approximations. Other approaches introduce the idea of critical points along the surfaces of obstacles [20, 27], which in turn results in control discontinuities due to the considerations of discrete proximity points. Furthermore, some require optimization algorithms that may not yield control torques in closed form [27].

Similar to the use of artificial potential field functions, recent efforts have proposed the concept of control barrier functions [31]. The aim is to design real-time controllers that keep the robot trajectories within a safety set [32]. These approaches, however, tend to be based on similar conservative ideas, such as the approximation of obstacles as spheres [33] or approximations of the shortest distance which yield nonsmooth controllers [34].

Recently, the use of ML methods to approximate the shape, shortest distance to collision, or safe boundaries has been proposed. For instance, in ref. [35], the authors propose a computationally efficient signed distance-based avoidance control [36] where the self-collision boundary is approximated using neural networks. Similarly, [37] presents a fast method to learn the shortest distance from the robot to an obstacle as a neural joint space implicit distance function. Yet, as is the case of most ML-based avoidance control methods, these techniques cannot rigorously guarantee stability and safety at all times.

1.2. Contributions

In this paper, we propose a decentralized, cooperative artificial potential field method based on avoidance functions for rigid manipulators. The control law is decentralized since only information from

other robots and obstacles within a bounded predefined distance needs to be considered and cooperative, given that it can guarantee collision avoidance at all times if other robots and dynamics obstacles abide by the same control policy [38]. The novelty of the approach is the proposal of a shape- and orientation-dependent, continuously differentiable safety minimum distance between two links or obstacles that yield continuous, closed-form controllers. The safety distance is a smooth analytical function that does not require optimization or discrete algorithms and which derivatives can be computed offline. The use of a continuous differentiable shortest distance eliminates the discontinuity of defining critical points or the conservatism of assuming spherical or ellipsoidal shapes. Moreover, our approach provides the development of closed-form analytical control input torques that are smooth and well defined. We prove, via Lyapunov analysis, that the cooperative control strategy guarantees the safety of the robotic manipulators at all times. We then provide explicit distance continuously differentiable formulas for manipulators with cylindrical links as well as simulations for two- and three-dimensional manipulators that illustrate the performance and efficacy of the proposed approach in comparison to the traditional use of spherical approximations. Finally, we formulate extensions of the proposed collision avoidance framework to other Lyapunov-based controllers, trajectory tracking controllers, and robotic systems with bounded control torques.

2. Preliminaries

2.1. Robot kinematics

We consider the task of safely coordinating the motion of N n_i-DOF rigid, nonlinear manipulators with generalized coordinates (or joint configurations) given by:

$$\mathbf{q}_i(t) = [q_{i1}(t), \cdots, q_{in_i}(t)]^T, \qquad \text{for } i \in \mathbb{N} \qquad (1)$$

where $\mathbb{N} = \{1, \cdots, N\}$ denotes the set of robots. The joints and links are labeled in ascending order from the most proximal to the most distal, as shown in Fig. 1. The position of the geometric center of each link with respect to a common world reference frame is denoted in Cartesian coordinates by $\mathbf{p}_{ij}(t) := \mathbf{p}_{ij}(\mathbf{q}_i(t)) \in \mathbb{R}^n$, where n is the dimension of the robots' workspace. The joint velocity $\dot{\mathbf{q}}_i(t)$ and the velocity of the geometric center $\dot{\mathbf{p}}_{ij}(t)$ are related by the translational Jacobian J_{ij}:

$$\dot{\mathbf{p}}_{ij}(t) = J_{ij}(\mathbf{q}_i(t))\dot{\mathbf{q}}_i(t), \qquad\qquad J_{ij}(\mathbf{q}_i(t)) = \frac{\partial \mathbf{p}_{ij}(t)}{\partial \mathbf{q}_i(t)}. \qquad (2)$$

In addition, we define the angular orientation of each link with respect to the common world frame as:

$$\boldsymbol{\theta}_{ij}(t) := [\phi_{ij}(\mathbf{q}_i(t)), \vartheta_{ij}(\mathbf{q}_i(t)), \psi_{ij}(\mathbf{q}_i(t))]^T \qquad (3)$$

where ϕ_{ij}, ϑ_{ij}, and ψ_{ij} denote the orientation of ith robot's jth link in Euler angles with respect to the xy, zx, and yz planes (or, equivalently, about the z, y, and x axes), respectively. Similar to the linear velocities, the angular velocities are related to joint velocities by the rotational Jacobian $\mathcal{J}_{ij}$:

$$\dot{\boldsymbol{\theta}}_{ij}(t) = \mathcal{J}_{ij}(\mathbf{q}_i(t))\dot{\mathbf{q}}_i(t), \qquad\qquad \mathcal{J}_{ij}(\mathbf{q}_i(t)) = \frac{\partial \boldsymbol{\theta}_{ij}(t)}{\partial \mathbf{q}_i(t)}. \qquad (4)$$

Note that in the case of planar manipulators, that is, $n = 2$, only one angular orientation is required. In what follows, we will omit the time argument of signals.

2.2. Robot dynamics

The manipulators are assumed to be fully actuated with nonlinear Lagrangian dynamics given by:

$$M_i(\mathbf{q}_i)\ddot{\mathbf{q}}_i + C_i(\mathbf{q}_i, \dot{\mathbf{q}}_i)\dot{\mathbf{q}}_i + \mathbf{g}_i(\mathbf{q}_i) = \boldsymbol{\tau}_i, \qquad i \in \mathbb{N} \qquad (5)$$

where $M_i(\mathbf{q}_i) \in \mathbb{R}^{n_i \times n_i}$ are the positive definite inertia matrices, $C_i(\mathbf{q}_i, \dot{\mathbf{q}}_i) \in \mathbb{R}^{n_i \times n_i}$ are the matrices of Coriolis and centrifugal terms, $\mathbf{g}_i(\mathbf{q}_i) = [g_{i1}(\mathbf{q}_i), \cdots, g_{in_i}(\mathbf{q}_i)]^T$ are the gravitational torques and forces, and $\boldsymbol{\tau}_i = [\tau_{i1}, \cdots, \tau_{in_i}]^T$ are the control inputs for the ith robot. We assume that $\mathbf{g}_i(\mathbf{q}_i) \in \mathbb{R}^{n_i}$ are known and, therefore, can be compensated via active control and that the manipulators satisfy the following standard properties for all $\mathbf{q}_i$ and $\dot{\mathbf{q}}_i$ [39].

Property 1. $\exists \overline{m}_i \geq \underline{m}_i > 0$ *such that* $\underline{m}_i \leq \|M(\mathbf{q}_i)\| \leq \overline{m}_i$.

Property 2. $\dot{M}_i(\mathbf{q}_i) - 2C_i(\mathbf{q}_i, \dot{\mathbf{q}}_i)$ *is skew-symmetric.*

2.3. Control objective

For simplicity, we assume that the links can be approximated (or enclosed by elongated convex shapes, as shown in Fig. 1. Furthermore, we assume that adjacent links (i.e., those that share a joint) are offset from each other, which implies that they can move freely without colliding. Using the geometric centers as reference points, we define a minimum safe distance between two nonadjacent links, $\mathbf{p}_{ij}$ and $\mathbf{p}_{kl}$, as:

$$r_{ij}^{kl} := r_{ij}^{kl}(\mathbf{p}_{ij}, \mathbf{p}_{kl}, \boldsymbol{\theta}_{ij}, \boldsymbol{\theta}_{kl}) = r_{kl}^{ij}, \qquad \text{for } k \in \mathbb{N}, l \in \mathbb{L}_{ij}^k \qquad (6)$$

where r_{ij}^{kl} is a continuous, differentiable function of the links' positions, orientations, and systems geometrical parameters, including length, depth, and width, and where

$$\mathbb{L}_{ij}^k := \{l \in \{1, \cdots, n_k\} \mid k \in \mathbb{N}/i\} \cup \{l \in \{1, \cdots, n_i\}/\{j-1, j, j+1\} \mid k = i\} \qquad (7)$$

represents the set of all nonadjacent links to the ith robot's jth link. It is assumed that this minimum safe distance is known or that it can be approximated from above. Then, we can formulate the control objective as follows. Design $\boldsymbol{\tau}_i$ such that $\|\mathbf{p}_{ij} - \mathbf{p}_{kl}\| > r_{ij}^{kl} \, \forall \, t \geq 0, j \in \{1, \cdots, n_i\}, k \in \mathbb{N}, l \in \mathbb{L}_{ij}^k$.

2.4. Approximation functions

In what follows, we make use of the following continuous differentiable functions to approximate the minimum, the maximum, and the absolute value functions. Let $\{a_1, \cdots, a_m, \varepsilon, \delta\}$ be a set of positive scalar constants. Then, the following functions

$$\tilde{\lambda}_\delta(a_1, \cdots, a_m) := \left(\sum_{i=1}^m a_i^{-\delta} \right)^{-\frac{1}{\delta}} \geq \min\{a_1, \cdots, a_m\} \qquad (8)$$

$$\tilde{\Lambda}_\delta(a_1, \cdots, a_m) := \left(\frac{1}{m} \sum_{i=1}^m a_i^{\delta} \right)^{\frac{1}{\delta}} \leq \max\{a_1, \cdots, a_m\} \qquad (9)$$

$$\tilde{\alpha}_\varepsilon(a_1) := \sqrt{a_1^2 + \varepsilon^2} = \tilde{\alpha}_\varepsilon(-a_1) > |a_1| \qquad (10)$$

are approximations of the minimum (from above), maximum (from below) [40], and absolute value (from above). Moreover, note that $\tilde{\lambda}_\delta(\cdot) \to \min\{\cdot\}$, $\tilde{\Lambda}_\delta(\cdot) \to \max\{\cdot\}$, and $\tilde{\alpha}_\varepsilon(\cdot) \to |\cdot|$ when $\delta \to \infty$ and $\varepsilon \to 0$.

3. Collision avoidance control

3.1. Avoidance functions

We use the concept of avoidance control [21, 38] and define an avoidance function, $V_{ij}^{kl} := V_{ij}^{kl}(\mathbf{p}_{ij}, \mathbf{p}_{kl}, r_{ij}^{kl})$, between two nonadjacent links as:

$$V_{ij}^{kl} := \left(\min \left\{ 0, \frac{\|\mathbf{p}_{ij} - \mathbf{p}_{kl}\|^2 - (r_{ij}^{kl} + \rho_{ij}^{kl})^2}{\|\mathbf{p}_{ij} - \mathbf{p}_{kl}\|^2 - (r_{ij}^{kl})^2} \right\} \right)^2 \qquad (11)$$

where $\rho_{ij}^{kl} = \rho_{kl}^{ij} > 0$ is a constant parameter. Herein, the term $r_{ij}^{kl} + \rho_{ij}^{kl}$ represents the distance at which the ith robot's jth link should start avoiding the kth robot's lth link. Note that $V_{ij}^{kl} = 0 \; \forall \; \|\mathbf{p}_{ij} - \mathbf{p}_{kl}\| \geq r_{ij}^{kl} + \rho_{ij}^{kl}$, $V_{ij}^{kl} \to \infty$ as $\|\mathbf{p}_{ij} - \mathbf{p}_{kl}\| \to r_{ij}^{kl}$, and its gradient with respect to $\mathbf{p}_i$ and r_{ij}^{kl} are

$$
\begin{bmatrix} \dfrac{\partial V_{ij}^{kl^T}}{\partial \mathbf{p}_{ij}} \\[2mm] \dfrac{\partial V_{ij}^{kl}}{\partial r_{ij}^{kl}} \end{bmatrix} = \begin{cases} f_{ij}^{kl} \begin{bmatrix} \mathbf{p}_{kl} - \mathbf{p}_{ij} \\[1mm] 2r_{ij}^{kl}\rho_{ij}^{kl} + \rho_{ij}^{kl^2} + \|\mathbf{z}_i - \mathbf{z}_j\|^2 \end{bmatrix} & \text{if } \|\mathbf{p}_{ij} - \mathbf{p}_{kl}\| \in (r_{ij}^{kl}, r_{ij}^{kl} + \rho_{ij}^{kl}) \\[4mm] \text{undefined}, & \text{if } \|\mathbf{p}_{ij} - \mathbf{p}_{kl}\| = r_{ij}^{kl} \\[2mm] \mathbf{0}^T, & \text{otherwise} \end{cases} \tag{12}
$$

where

$$
f_{ij}^{kl} = 4\rho_{ij}^{kl} \left(\left(r_{ij}^{kl} + \rho_{ij}^{kl}\right)^2 - \|\mathbf{p}_{ij} - \mathbf{p}_{kl}\|^2 \right) \left(\|\mathbf{p}_{ij} - \mathbf{p}_{kl}\|^2 - \left(r_{ij}^{kl}\right)^2 \right)^{-3}. \tag{13}
$$

Furthermore, one can show that V_{ij}^{kl} is almost everywhere continuously differentiable that

$$
\frac{\partial V_{ij}^{kl}}{\partial \mathbf{p}_{ij}} = \frac{\partial V_{kl}^{ij}}{\partial \mathbf{p}_{ij}} = -\frac{\partial V_{ij}^{kl}}{\partial \mathbf{p}_{kl}} = -\frac{\partial V_{kl}^{ij}}{\partial \mathbf{p}_{kl}}, \qquad\qquad \frac{\partial V_{ij}^{kl}}{\partial r_{ij}^{kl}} = \frac{\partial V_{kl}^{ij}}{\partial r_{kl}^{ij}} \tag{14}
$$

and that

$$
\begin{aligned}
\frac{1}{2}\sum_{i=1}^{N}\sum_{j=1}^{n_i}\sum_{k=1}^{N}\sum_{l\in\mathbb{L}_{ij}^k} \dot{V}_{ij}^{kl} &= \frac{1}{2}\sum_{i=1}^{N}\sum_{j=1}^{n_i}\sum_{k=1}^{N}\sum_{l\in\mathbb{L}_{ij}^k} \left(\frac{\partial V_{ij}^{kl}}{\partial \mathbf{p}_{ij}}\frac{\partial \mathbf{p}_{ij}}{\partial \mathbf{q}_i}\dot{\mathbf{q}}_i + \frac{\partial V_{ij}^{kl}}{\partial r_{ij}^{kl}}\frac{\partial r_{ij}^{kl}}{\partial \mathbf{p}_{ij}}\frac{\partial \mathbf{p}_{ij}}{\partial \mathbf{q}_i}\dot{\mathbf{q}}_i + \frac{\partial V_{ij}^{kl}}{\partial r_{ij}^{kl}}\frac{\partial r_{ij}^{kl}}{\partial \boldsymbol{\theta}_{ij}}\frac{\partial \boldsymbol{\theta}_{ij}}{\partial \mathbf{q}_i}\dot{\mathbf{q}}_i \right. \\[2mm]
&\quad \left. + \frac{\partial V_{kl}^{ij}}{\partial \mathbf{p}_{kl}}\frac{\partial \mathbf{p}_{kl}}{\partial \mathbf{q}_k}\dot{\mathbf{q}}_k + \frac{\partial V_{kl}^{ij}}{\partial r_{kl}^{ij}}\frac{\partial r_{kl}^{ij}}{\partial \mathbf{p}_{kl}}\frac{\partial \mathbf{p}_{kl}}{\partial \mathbf{q}_k}\dot{\mathbf{q}}_k + \frac{\partial V_{kl}^{ij}}{\partial r_{kl}^{ij}}\frac{\partial r_{kl}^{ij}}{\partial \boldsymbol{\theta}_{kl}}\frac{\partial \boldsymbol{\theta}_{kl}}{\partial \mathbf{q}_k}\dot{\mathbf{q}}_k \right) \\[2mm]
&= \sum_{i=1}^{N}\sum_{j=1}^{n_i}\sum_{k=1}^{N}\sum_{l\in\mathbb{L}_{ij}^k} \left(\frac{\partial V_{ij}^{kl}}{\partial \mathbf{p}_{ij}}J_{ij} + \frac{\partial V_{ij}^{kl}}{\partial r_{ij}^{kl}}\frac{\partial r_{ij}^{kl}}{\partial \mathbf{p}_{ij}}J_{ij} + \frac{\partial V_{ij}^{kl}}{\partial r_{ij}^{kl}}\frac{\partial r_{ij}^{kl}}{\partial \boldsymbol{\theta}_{ij}}\mathcal{J}_{ij} \right) \dot{\mathbf{q}}_i. \tag{15}
\end{aligned}
$$

Note that in contrast to other definitions of avoidance functions [23, 38], the ones defined here use a nonconstant safe distance radius.

3.2. Control law

Herein, we will consider the control task of achieving a desired, constant joint configuration, $\mathbf{q}_i^d \in \mathbb{R}^{n_i}$, while avoiding collisions. Accordingly, we propose a proportional derivative (PD) control law with gravity compensation and collision avoidance given by:

$$
\boldsymbol{\tau}_i = \mathbf{g}_i - A_i(\mathbf{q}_i - \mathbf{q}_i^d) - B_i\dot{\mathbf{q}}_i - \sum_{j=1}^{n_i}\sum_{k=1}^{N}\sum_{l\in\mathbb{L}_{ij}^k} \mathbf{u}_{ij}^{kl} \tag{16a}
$$

$$
\mathbf{u}_{ij}^{kl} = J_{ij}^T \left(\frac{\partial V_{ij}^{kl}}{\partial \mathbf{p}_{ij}} + \frac{\partial V_{ij}^{kl}}{\partial r_{ij}^{kl}}\frac{\partial r_{ij}^{kl}}{\partial \mathbf{p}_{ij}} \right)^T + \mathcal{J}_{ij}^T \left(\frac{\partial V_{ij}^{kl}}{\partial r_{ij}^{kl}}\frac{\partial r_{ij}^{kl}}{\partial \boldsymbol{\theta}_{ij}} \right)^T \tag{16b}
$$

where $\mathbf{u}_{ij}^{kl} \in \mathbb{R}^{n_i}$ represents the avoidance control torque generated by the interaction between the ith robot's jth link and the kth robot's lth link and where $A_i = \text{diag}(a_{i1}, \cdots, a_{in_i})$ and $B_i = \text{diag}(b_{i1}, \cdots, b_{in_i})$ are positive-definite, diagonal matrices. As it will be shown next, the closed-loop control law (16) guarantees a safe minimum distance among nonadjacent links at all times.

Proposition 1 (Collision Avoidance). *Consider a group of N n_i-DOF manipulators with dynamics and control inputs given by (5) and (16). Assume that $\|\mathbf{p}_{ij}(0) - \mathbf{p}_{kl}(0)\| > r_{ij}^{kl}$ for all $i, k \in \mathbb{N}$, $j \in \{1, \cdots, n_i\}$, $l \in \mathbb{L}_{ij}^k$. Then, $\|\mathbf{p}_{ij}(t) - \mathbf{p}_{kl}(t)\| > r_{ij}^{kl} \; \forall \; t \geq 0$.*

Proof. Consider the Lyapunov candidate function:

$$\mathcal{V} = \frac{1}{2}\sum_{i=1}^{N}\left((\mathbf{q}_i - \mathbf{q}_i^d)^T A_i(\mathbf{q}_i - \mathbf{q}_i^d) + \dot{\mathbf{q}}_i^T M_i \dot{\mathbf{q}}_i\right) + \frac{1}{2}\sum_{i=1}^{N}\sum_{j=1}^{n_i}\sum_{k=1}^{N}\sum_{l\in\mathbb{L}_{ij}^k} V_{ij}^{kl} \tag{17}$$

which is positive for all $[\mathbf{q}_i - \mathbf{q}_i^d, \dot{\mathbf{q}}_i]^T \neq \mathbf{0}$ (from Property 1). Taking its time derivative and using equations (5), (15), and (16) yields

$$\dot{\mathcal{V}} = \sum_{i=1}^{N}\left((\mathbf{q}_i - \mathbf{q}_i^d)^T A_i \dot{\mathbf{q}}_i + \dot{\mathbf{q}}_i^T\left(M_i\ddot{\mathbf{q}}_i + \frac{\dot{M}_i}{2}\dot{\mathbf{q}}_i\right)\right) + \sum_{i=1}^{N}\sum_{j=1}^{n_i}\sum_{k=1}^{N}\sum_{l\in\mathbb{L}_{ij}^k}\left(\frac{\partial V_{ij}^{kl}}{\partial \mathbf{p}_{ij}}J_{ij} + \frac{\partial V_{ij}^{kl}}{\partial r_{ij}^{kl}}\left(\frac{\partial r_{ij}^{kl}}{\partial \mathbf{p}_{ij}}J_{ij} + \frac{\partial r_{ij}^{kl}}{\partial \boldsymbol{\theta}_{ij}}\mathcal{J}_{ij}\right)\right)\dot{\mathbf{q}}_i$$

$$= \sum_{i=1}^{N}\left((\mathbf{q}_i - \mathbf{q}_i^d)^T A_i \dot{\mathbf{q}}_i - \dot{\mathbf{q}}_i^T\left(C_i\dot{\mathbf{q}}_i + A_i(\mathbf{q}_i - \mathbf{q}_i^d) + B_i\dot{\mathbf{q}}_i + \sum_{j=1}^{n_i}\sum_{k=1}^{N}\sum_{l\in\mathbb{L}_{ij}^k}\mathbf{u}_{ij}^{kl} + \frac{\dot{M}_i}{2}\dot{\mathbf{q}}_i\right)\right)$$

$$+ \sum_{i=1}^{N}\sum_{j=1}^{n_i}\sum_{k=1}^{N}\sum_{l\in\mathbb{L}_{ij}^k}\mathbf{u}_{ij}^{kl^T}\dot{\mathbf{q}}_i = -\sum_{i=1}^{N}\dot{\mathbf{q}}_i^T B_i \dot{\mathbf{q}}_i + \frac{1}{2}\sum_{i=1}^{N}\dot{\mathbf{q}}_i^T(\dot{M} - 2C_i)\dot{\mathbf{q}}_i = -\sum_{i=1}^{N}\dot{\mathbf{q}}_i^T B_i \dot{\mathbf{q}}_i \tag{18}$$

where we used Property 2. Since $\dot{\mathcal{V}} \leq -\sum_{i=1}^{N}\underline{b}_i\left\|\dot{\mathbf{q}}_i\right\|^2 \leq 0$, where $\underline{b}_i > 0$ is the smallest eigenvalue of B_i, we have that $\mathcal{V}$ is non-increasing and bounded by $\mathcal{V}(0)$ for all $t \geq 0$. Now, suppose that for some nonadjacent links $\left\|\mathbf{p}_{ij}(t) - \mathbf{p}_{kl}(t)\right\| \to r_{ij}^{kl}$ for some t. The latter would imply that $V_{ij}^{kl} \to \infty \Rightarrow \mathcal{V} \to \infty$, which is a contradiction. Since the solutions of equation (5) are continuous, one has that $\left\|\mathbf{p}_{ij}(t) - \mathbf{p}_{kl}(t)\right\| > r_{ij}^{kl}$ for all $t \geq 0$ and the proof is complete. □

3.3. Extensions, considerations, and limitations
3.3.1. Lyapunov-based controllers
It is worth noting that other closed-loop controllers can be used in place of a traditional PD-type control, including nonlinear controllers. For instance, consider a controller of the form:

$$\tau_i = \mathbf{g}_i - \frac{\partial \mathcal{A}_i}{\partial \mathbf{q}_i} - \frac{\partial \mathcal{B}_i}{\partial \dot{\mathbf{q}}_i} - \sum_{j=1}^{n_i}\sum_{k=1}^{N}\sum_{l\in\mathbb{L}_{ij}^k}\mathbf{u}_{ij}^{kl} \tag{19}$$

where $\mathcal{A}_i := \mathcal{A}_i(\mathbf{q}_i - \mathbf{q}_i^d)$ and $\mathcal{B}_i := \mathcal{B}_i(\dot{\mathbf{q}}_i)$ are functions with the following properties:

- $\mathcal{A}_i$ is positive-definite, that is, $\mathcal{A}_i = 0$ for $\mathbf{q}_i - \mathbf{q}_i^d = \mathbf{0}$ and $\mathcal{A}_i > 0$ otherwise.
- $\mathcal{A}_i$ is radially unbounded, that is, $\mathcal{A}_i \to \infty$ if $\left\|\mathbf{q}_i - \mathbf{q}_i^d\right\| \to \infty$.
- $(\partial \mathcal{B}_i/\partial \dot{\mathbf{q}}_i)\dot{\mathbf{q}}_i \geq 0 \,\forall \dot{\mathbf{q}}_i$.

Then, following the steps of the proof of Proposition 1, one can show that the time derivative of the following candidate Lyapunov function

$$\overline{\mathcal{V}}_i = \frac{1}{2}\sum_{i=1}^{N}\left(\mathcal{A}_i + \dot{\mathbf{q}}_i^T M_i \dot{\mathbf{q}}_i\right) + \frac{1}{2}\sum_{i=1}^{N}\sum_{j=1}^{n_i}\sum_{k=1}^{N}\sum_{l\in\mathbb{L}_{ij}^k}u_{ij}^{kl} \tag{20}$$

is $\dot{\overline{\mathcal{V}}}_i = -\sum_{i=1}^{N}(\partial \mathcal{B}_i/\partial \dot{\mathbf{q}}_i)\dot{\mathbf{q}}_i \leq 0$ and the same statements from Proposition 1 will hold.

Note that the PD-type controller in (16a) belongs to this class controllers with $\mathcal{A}_i = (\mathbf{q}_i - \mathbf{q}_i^d)^T A_i(\mathbf{q}_i - \mathbf{q}_i^d)$ and $\mathcal{B}_i = \dot{\mathbf{q}}_i^T B_i \dot{\mathbf{q}}_i$.

3.3.2. Trajectory tracking

The analysis performed in this section assumes a desired constant configuration $\dot{\mathbf{q}}_i^d \equiv 0$. However, many applications require the robotic manipulator to move along a trajectory. Therefore, let's consider a desired trajectory $(\mathbf{q}_i^d, \dot{\mathbf{q}}_i^d, \ddot{\mathbf{q}}_i^d)$ along with an inverse dynamics controller of the form:

$$\tau_i = M_i \ddot{\mathbf{q}}_i^d + C_i \dot{\mathbf{q}}_i^d + \mathbf{g}_i - A_i(\mathbf{q}_i - \mathbf{q}_i^d) - B_i(\dot{\mathbf{q}}_i - \dot{\mathbf{q}}_i^d) - \sum_{j=1}^{n_i} \sum_{k=1}^{N} \sum_{l \in \mathbb{L}_{ij}^k} \mathbf{u}_{ij}^{kl}. \tag{21}$$

Substituting (21) into (1) yields

$$M_i \ddot{\tilde{\mathbf{q}}}_i + C_i \dot{\tilde{\mathbf{q}}}_i = -A_i \tilde{\mathbf{q}}_i - B_i \dot{\tilde{\mathbf{q}}}_i - \sum_{j=1}^{n_i} \sum_{k=1}^{N} \sum_{l \in \mathbb{L}_{ij}^k} \mathbf{u}_{ij}^{kl} \tag{22}$$

where $\tilde{\mathbf{q}}_i = \mathbf{q}_i - \mathbf{q}_i^d$. Then, the following result about collision avoidance follows.

Proposition 2 (Collision Avoidance with Trajectory Tracking). *Consider a group of N n_i-DOF manipulators with feedback dynamics given by (22). Assume that $\left\| \mathbf{p}_{ij}(0) - \mathbf{p}_{kl}(0) \right\| > r_{ij}^{kl}$ for all $i, k \in \mathbb{N}$, $j \in \{1, \cdots, n_i\}$, $l \in \mathbb{L}_{ij}^k$ and that desired trajectory chosen such that the following inequality is satisfied*

$$\underline{b}_i \left\| \dot{\tilde{\mathbf{q}}}_i \right\|^2 + \dot{\mathbf{q}}_i^{d^T} \sum_{j=1}^{n_i} \sum_{k=1}^{N} \sum_{l \in \mathbb{L}_{ij}^k} \mathbf{u}_{ij}^{kl} \geq 0, \qquad \qquad \forall\, i \in \{1, \cdots, N\}. \tag{23}$$

Then, $\left\| \mathbf{p}_{ij}(t) - \mathbf{p}_{kl}(t) \right\| > r_{ij}^{kl}\ \forall\, t \geq 0$.

Proof. The proof follows similar to the steps from Proposition 1. Consider the following Lyapunov candidate function:

$$\tilde{\mathcal{V}} = \frac{1}{2} \sum_{i=1}^{N} \left(\tilde{\mathbf{q}}_i^T A_i \tilde{\mathbf{q}}_i + \dot{\tilde{\mathbf{q}}}_i^T M_i \dot{\tilde{\mathbf{q}}}_i \right) + \frac{1}{2} \sum_{i=1}^{N} \sum_{j=1}^{n_i} \sum_{k=1}^{N} \sum_{l \in \mathbb{L}_{ij}^k} V_{ij}^{kl}. \tag{24}$$

Taking its time derivative, one obtains

$$\dot{\tilde{\mathcal{V}}} = -\sum_{i=1}^{N} \dot{\tilde{\mathbf{q}}}_i^T B_i \dot{\tilde{\mathbf{q}}}_i - \sum_{i=1}^{N} \sum_{j=1}^{n_i} \sum_{k=1}^{N} \sum_{l \in \mathbb{L}_{ij}^k} (\dot{\mathbf{q}}_i - \dot{\mathbf{q}}_i^d)^T \mathbf{u}_{ij}^{kl} + \sum_{i=1}^{N} \sum_{j=1}^{n_i} \sum_{k=1}^{N} \sum_{l \in \mathbb{L}_{ij}^k} \mathbf{u}_{ij}^{kl^T} \dot{\mathbf{q}}_i$$

$$\leq -\sum_{i=1}^{N} \left(\underline{b}_i \left\| \dot{\tilde{\mathbf{q}}}_i \right\|^2 + \sum_{j=1}^{n_i} \sum_{k=1}^{N} \sum_{l \in \mathbb{L}_{ij}^k} \dot{\mathbf{q}}_i^{d^T} \mathbf{u}_{ij}^{kl} \right) \leq 0 \tag{25}$$

where we used assumption (23). Since $\dot{\tilde{\mathcal{V}}}$ is nonpositive, one has that $\tilde{\mathcal{V}}$ is non-increasing and bounded. Using similar arguments as in Proposition 1, one can finally conclude that a collision cannot take place. $\qquad \square$

Note that (23) is always satisfied for $\dot{\mathbf{q}}_i = 0$. Therefore, to avoid violation of (23), one can alternatively freeze the desired trajectory until the conflict is resolved as proposed in ref. [41]. It is also worth noting that the inverse dynamics control law (21) requires accurate estimation of the system parameters, and so does (16) for the compensation of the gravitational torques. In ref. [42], the authors discuss adaptive and robust inverse dynamics control laws that can be applied in lieu of (21) with little alteration to the collision avoidance results. Similarly, the work in ref. [43] summarizes different system identification methods for robotics manipulators that could be combined with the proposed avoidance control.

3.3.3. Path planning

The proposed minimum safe distance approach has been formulated for real-time, reactive collision avoidance control laws. It is a function of the agents' relative position, orientation, and shapes. The proposed formulation of the minimum distance can potentially be adapted to path planning algorithms that employ potential field functions similar to the work in refs. [10, 25]. Yet, the time-varying property of the minimum safe distance, which molds the shape of the artificial potential field functions, adds another degree of complexity to the path planning problem. The latter is particularly significant if obstacles in the robot's environment are also moving.

3.3.4. Deadlocks

A deadlock or an unwanted local minimum refers to the convergence of the manipulator to a configuration different from the desired one. This is a common drawback of decentralized motion planning algorithms and potential field methods, including the one proposed in this paper. Conventional solutions to help avoid or escape deadlocks include changing, at least temporarily, the desired configuration when a deadlock is reached or adding a perturbation control torque to (16) as in ref. [44]. Yet, none of these methods can guarantee with certainty that the robot will not return to a deadlock.

3.3.5. Dynamic obstacles

The proposed control law is cooperative, meaning that it assumes that all other robots apply the same avoidance control. The results of collision avoidance naturally extend to static obstacles of any shape, given that their velocities are zero. Problems may arise when interacting with dynamic obstacles, for which collision avoidance is, in general, not guaranteed. For instance, a manipulator with a stationary base cannot avoid a collision with an approaching obstacle. Similarly, a manipulator trapped in a deadlock might not be able to resolve the conflict with other noncooperative, fast-moving objects. Yet, the use of artificial potential field functions has been shown to be robust against non-threatening, slow-moving dynamic obstacles [44]. The work in ref. [45] presents sufficient conditions for avoidance control laws based on artificial potential field-like functions.

3.3.6. Kinematic and dynamic constraints

Of practical interest is the consideration of kinematic and dynamic constraints, such as joint and control torque limits. Joint limitations can be handled as obstacles that move with the links and, in general, may not represent a threat of collision when interacting with cooperative objects, as these other robots or links will aim to avoid a collision. Dynamic constraints, on the other hand, can be handled by careful consideration of the control law. For example, consider a group of robotic manipulators with bounded control torques, that is, $\exists T_{ij} \in (0, \infty)$ such that $|\tau_{ij}| \leq T_{ij}$ for all $i \in \{i, \cdots, N\}$, $j \in \{1, \cdots, n_i\}$. In addition, assume that the gravity torques are also bounded, that is, $\exists G_{ij} \in [0, \infty)$ such that $|g_{ij}| \leq G_{ij}$. The latter property is satisfied by a wide range of robotic manipulators, including those with only revolute joints [46]. Now, consider the following saturated control PD-type controller with gravity compensation:

$$\tau_i = \mathbf{g}_i - \mathbf{sat}_i \left(A_i \tilde{\mathbf{q}}_i + B_i \dot{\mathbf{q}}_i \right), \qquad \mathrm{sat}_{ij}(a) = \begin{cases} a, & \text{if } |a| \leq \omega_{ij} \\ \omega_{ij} \frac{a}{|a|}, & \text{otherwise} \end{cases} \qquad (26)$$

where $\mathbf{sat}_i(\cdot) = [\mathrm{sat}_{i1}(\cdot), \cdots, \mathrm{sat}_{in_i}(\cdot)]^T$ is the saturation function and $0 < \omega_{ij} \leq T_{ij} - G_{ij}$ are some control parameters. Note that $|\tau_{ij}| \leq T_i \,\forall\, i, j$. Consider then the following positive-definite function:

$$\mathcal{W}_i = \frac{1}{2} \dot{\mathbf{q}}_i^T M_i \dot{\mathbf{q}}_i + \int_0^{\tilde{\mathbf{q}}_i} \mathbf{sat}_i(A_i \mathbf{r}) d\mathbf{r}. \qquad (27)$$

In ref. [47], it is shown that $\dot{\mathcal{W}}_i \leq 0 \;\forall\; t \geq 0$ and that $\mathbf{q}_i \to \mathbf{q}_i^d$, $\dot{\mathbf{q}}_i \to \mathbf{0}$ as $t \to \infty$. Using these results, one can prove the following statement.

Proposition 3 (Collision Avoidance with Bounded Inputs). *Consider a group of N n_i-DOF manipulators with control input given by:*

$$\tau_i = \mathbf{g}_i - \mathbf{sat}_i\left(A_i\tilde{\mathbf{q}}_i + B_i\dot{\mathbf{q}}_i\right) - \sum_{j=1}^{n_i}\sum_{k=1}^{N}\sum_{l\in\mathbb{L}_{ij}^k}\mathbf{u}_{ij}^{kl} \tag{28}$$

and define

$$\bar{u}_{ij} := \mathbf{e}_j^T \sum_{j=1}^{n_i}\sum_{k=1}^{N}\sum_{l\in\mathbb{L}_{ij}^k}\mathbf{u}_{ij}^{kl} \tag{29}$$

as the ith robot's jth joint's total avoidance control law, where $\mathbf{e}_j$ is the zero vector with jth element 1. Assume that $\left\|\mathbf{p}_{ij}(0) - \mathbf{p}_{kl}(0)\right\| > r_{ij}^{kl}$ for all $i, k \in \mathbb{N}$, $j \in \{1, \cdots, n_i\}$, $l \in \mathbb{L}_{ij}^k$ and that

$$|\bar{u}_{ij}| \leq U_{ij} = T_{ij} - G_{ij} - \omega_{ij}, \qquad\qquad \forall\; i,j. \tag{30}$$

Then, $|\tau_{ij}| \leq T_{ij}$ and $\left\|\mathbf{p}_{ij}(t) - \mathbf{p}_{kl}(t)\right\| > r_{ij}^{kl} \;\forall\; t \geq 0$.

Proof. The first statement follows from

$$|\tau_{ij}| \leq |g_{ij}| + |\text{sat}_{ij}(a_{ij}(q_{ij} - q_{ij}^d) + b_{ij}\dot{q}_{ij})| + |u_{ij}| \leq G_{ij} + \omega_{ij} + U_{ij} \leq T_{ij}. \tag{31}$$

To prove the second statement, consider the following Lyapunov candidate function:

$$\mathcal{W} = \sum_{i=1}^{N}\mathcal{W}_i + \frac{1}{2}\sum_{i=1}^{N}\sum_{j=1}^{n_i}\sum_{k=1}^{N}\sum_{l\in\mathbb{L}_{ij}^k}V_{ij}^{kl}. \tag{32}$$

Following the steps of the proof of [47, Proposition 1], one can show that

$$\dot{\mathcal{W}}_i \leq -\sum_{j=1}^{n_i}\sum_{k=1}^{N}\sum_{l\in\mathbb{L}_{ij}^k}\mathbf{u}_{ij}^{kl^T}\dot{\mathbf{q}}_i \tag{33}$$
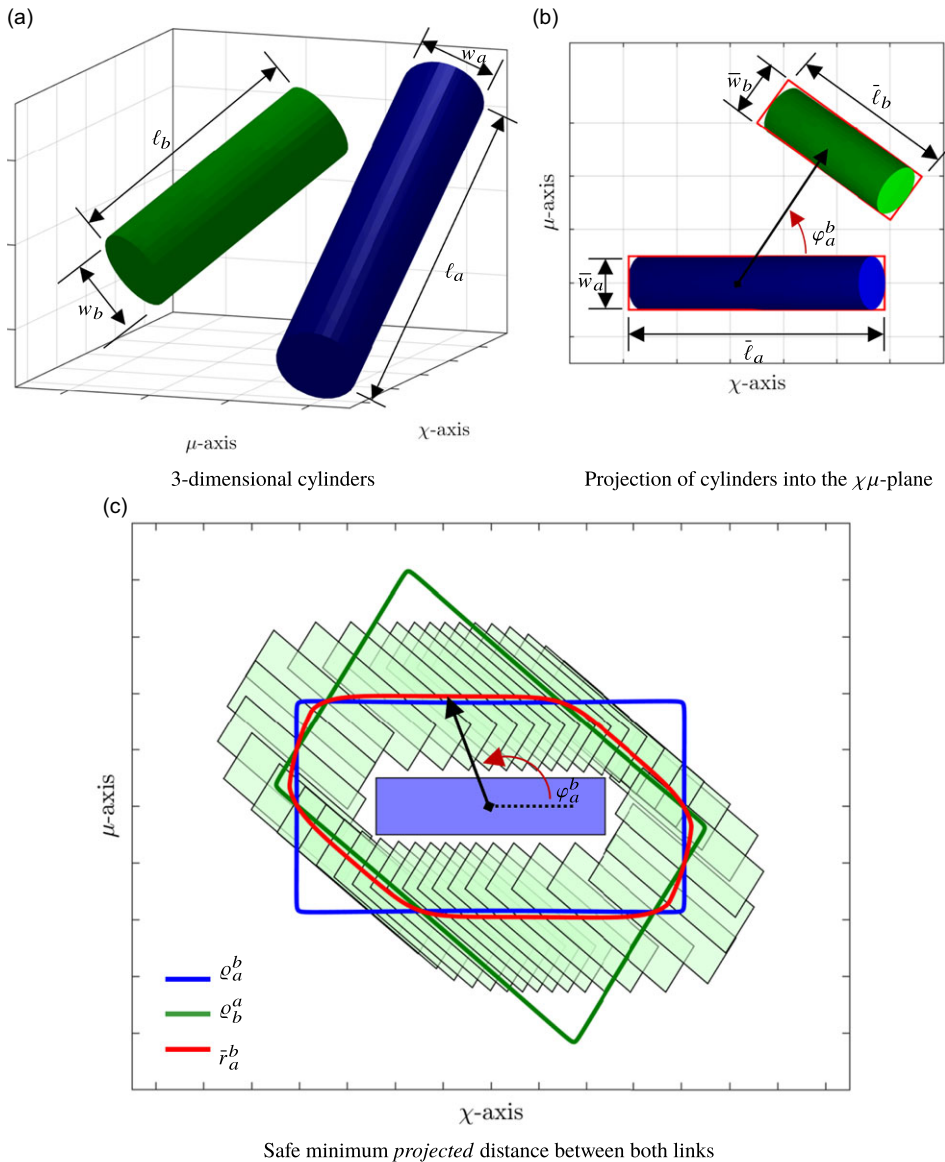
and, therefore

$$\dot{\mathcal{W}} = \sum_{i=1}^{N}\dot{\mathcal{W}}_i - \sum_{i=1}^{N}\sum_{j=1}^{n_i}\sum_{k=1}^{N}\sum_{l\in\mathbb{L}_{ij}^k}\mathbf{u}_{ij}^{kl^T}\dot{\mathbf{q}}_i \leq 0. \tag{34}$$

Using the same arguments as in Proposition 1, one can conclude that boundedness of $\mathcal{W}$ implies boundedness of V_{ij}^{kl}, which in turns implies collision avoidance at all times. $\square$

Note that assumption (30) cannot always be enforced and, therefore, collisions might not be averted at all times. The work in ref. [48] discusses alternative solutions that could potentially be adapted to robotic manipulators to guarantee collision avoidance in the presence of these control limitations. These include controlling the desired trajectory such that control bounds are enforced.

3.3.7. Computational complexity
The proposed avoidance control framework defines the avoidance (or potential field) functions (11) with respect to a state-dependent radius (6). Since the radius is not constant, the avoidance control input (16b) includes as extra terms the partial derivatives of the radius, which increases the complexity of the algorithm. However, these terms, which are a function of the dimensions of the links and objects as well as the position and orientation, can be given in closed form and do not have to be derived online. In addition, the multi-agent control algorithm has time complexity $O(N^2\bar{n}^2)$, where N is the number of

(a) 3-dimensional cylinders

(b) Projection of cylinders into the $\chi\mu$-plane

(c) Safe minimum *projected* distance between both links

Figure 2. *Projections of two cylinders in a plane and the minimum safe distance relative to their orientations.*

robots and $\bar{n}$ is the number of links per robot. In contrast, traditional artificial potential field functions that approximate links as an arrangement of spheres have a time complexity of $O(N^2\bar{n}_i^2 m^2)$, where m is the number of spheres per link.

4. Examples: n_i-manipulators with right cylindrical links

Herein, we will consider the case in which the links of the robotic manipulators can be approximated by right circular cylinders. Accordingly, consider two cylindrical bodies, namely the ath and bth links, as seen in Figure 2a. Let the lengths and diameters for the ath and bth links be given by (ℓ_a, w_a) and (ℓ_b, w_b),

respectively. We will now approximate the minimum safe distance of the link's rectangular projections in all three orthogonal planes, xy, yz, and zx.

For generality, consider an orthogonal $\chi\mu$-plane, where χ is the abscissa and μ is the ordinate (refer to Figure 2b). Let $\bar{\ell}_a$ and $\bar{\ell}_b$ be the projected lengths along the abscissa and $\overline{w}_a$ and $\overline{w}_b$ the projected widths for the ath and bth links. Define σ_a and σ_b as the orientations of the links with respect to the χ-axis and let

$$\beta_a^b := \beta(\bar{\ell}_a, \bar{\ell}_b, \overline{w}_b, \sigma_a, \sigma_b) = \frac{\bar{\ell}_a}{2} + \frac{\bar{\ell}_b}{2}\tilde{\alpha}_\varepsilon(\cos(\sigma_a - \sigma_b)) + \frac{\overline{w}_b}{2}\tilde{\alpha}_\varepsilon(\sin(\sigma_a - \sigma_b)) \tag{35a}$$

$$\gamma_a^b := \gamma(\bar{\ell}_b, \overline{w}_a, \overline{w}_b, \sigma_a, \sigma_b) = \frac{\overline{w}_a}{2} + \frac{\bar{\ell}_b}{2}\tilde{\alpha}_\varepsilon(\sin(\sigma_a - \sigma_b)) + \frac{\overline{w}_b}{2}\tilde{\alpha}_\varepsilon(\cos(\sigma_a - \sigma_b)) \tag{35b}$$

represent the combined length of the two links along the χ- and μ-axis, respectively, and where $\tilde{\alpha}_\varepsilon(\cdot)$ is the smooth approximation of the minimum function defined in (10). Moreover, let (χ_a, μ_a) and (χ_b, μ_b) be the coordinates of the ath and bth link's centers and define $\varphi_a^b = \operatorname{atan2}(\mu_b - \mu_a, \chi_b - \chi_a) - \sigma_a$ as the relative orientation of the bth link's center with respect to the ath link. Then, the equation of the rectangle with sides β_a^b and γ_a^b (rotated by σ_a) in polar coordinates $(\varrho_a^b, \varphi_a^b)$:

$$\zeta_a^b := \zeta(\bar{\ell}_a, \bar{\ell}_b, \overline{w}_a, \overline{w}_b, \sigma_a, \sigma_b, \varphi_a^b) = \tilde{\alpha}_\varepsilon(\gamma_a^b \cos\varphi_a^b + \beta_a^b \sin\varphi_a^b) \tag{36}$$

$$\eta_a^b := \eta(\bar{\ell}_a, \bar{\ell}_b, \overline{w}_a, \overline{w}_b, \sigma_a, \sigma_b, \varphi_a^b) = \tilde{\alpha}_\varepsilon(\gamma_a^b \cos\varphi_a^b - \beta_a^b \sin\varphi_a^b) \tag{37}$$

$$\varrho_a^b := \varrho(\bar{\ell}_a, \bar{\ell}_b, \overline{w}_a, \overline{w}_b, \sigma_a, \sigma_b, \varphi_a^b) = \frac{2\beta_a^b \gamma_a^b}{\zeta_a^b + \eta_a^b - 2\varepsilon} > 0. \tag{38}$$

Figure 2c shows a representation of ϱ_a^b as a function φ_a^b for fixed parameters $\bar{\ell}_a, \bar{\ell}_b, \overline{w}_a, \overline{w}_b, \sigma_a$, and σ_b. Now, let us repeat the process but from the perspective of the bth link. That is, compute $\beta_b^a := \beta(\bar{\ell}_b, \bar{\ell}_a, \overline{w}_a, \sigma_b, \sigma_a)$, $\gamma_b^a := \gamma(\bar{\ell}_b, \bar{\ell}_a, \overline{w}_a, \sigma_b, \sigma_a)$, $\zeta_b^a := \zeta(\bar{\ell}_b, \bar{\ell}_a, \overline{w}_b, \overline{w}_a, \sigma_b, \sigma_a, \varphi_b^a)$, $\eta_b^a := \eta(\bar{\ell}_b, \bar{\ell}_a, \overline{w}_b, \overline{w}_a, \sigma_b, \sigma_a, \varphi_b^a)$, and $\varrho_b^a := \varrho(\bar{\ell}_b, \bar{\ell}_a, \overline{w}_b, \overline{w}_a, \sigma_b, \sigma_a, \varphi_b^a)$ using equations (35)-(38), where $\varphi_b^a = \operatorname{atan2}(\mu_a - \mu_b, \chi_a - \chi_b) - \sigma_b$. This yields the equation in polar coordinates $(\varrho_b^a, \varphi_b^a)$ of the rectangle with sides β_b^a and γ_b^a, rotated by σ_b. Then, the minimum safe distance between the rectangular projection of both links in the $\chi\mu$-plane, denoted as $\bar{r}_a^b$, can be approximated from above by:

$$\bar{r}_a^b = \bar{r}_b^a = \tilde{\lambda}_\delta(\varrho_a^b, \varrho_b^a), \qquad\qquad \text{for some } \delta > 0 \tag{39}$$

where $\tilde{\lambda}_\delta$ is the approximation of the minimum function (8). Figure 2c illustrates how the minimum distance $\bar{r}_a^b$ changes in magnitude as a function of φ_a^b.

4.1. Example: 2D manipulators

Consider a group of N n_i-DOF planar manipulators in the xy-plane with link center coordinates $\mathbf{p}_{ij} = [x_{ij}, y_{ij}]^T \in \mathbb{R}^2$ and orientation $\boldsymbol{\theta}_{ij} = \phi_{ij} \in \mathbb{R}$. We assume that the links can be approximated by right circular cylinders with length $\ell_{ij} > 0$ and width $w_{ij} > 0$, with lengths aligned with the x-axis. Define distance formulas $\varrho_{ij}^{kl} := \varrho(\ell_{ij}, \ell_{kl}, w_{ij}, w_{kl}, \phi_{ij}, \phi_{kl}, \varphi_{ij}^{kl})$ and $\varrho_{kl}^{ij} := \varrho(\ell_{kl}, \ell_{ij}, w_{kl}, w_{ij}, \phi_{kl}, \phi_{ij}, \varphi_{kl}^{ij})$ using (38), where $\varphi_{ij}^{kl} = \operatorname{atan2}(y_{kl} - y_{ij}, x_{kl} - x_{ij}) - \phi_{ij}$ and $\varphi_{kl}^{ij} = \operatorname{atan2}(y_{ij} - y_{kl}, x_{ij} - x_{kl}) - \phi_{kl}$. Then, one can approximate the minimum safe radius from above as:

$$r_{ij}^{kl} = r_{kl}^{ij} = \tilde{\lambda}_\delta(\varrho_{ij}^{kl}, \varrho_{kl}^{ij}), \qquad\qquad \text{for some } \delta > 0. \tag{40}$$

To illustrate the performance of the control law, we now simulate the interaction of two distinct 4-DOF revolute planar manipulators with parameters listed in Table I, where m_{ij} denotes the mass of the ith robot's jth link. The manipulators implement the control law in (16), taking into account the safe interactions with a rigid wall at $y = 0$ (m) and the centers of each nonadjacent link. The control parameters are then given by $A_i = \operatorname{diag}(9, 6, 4, 4)$, $B_i = \operatorname{diag}(8, 8, 8, 8)$, $\rho_{ij}^{kl} = 0.25$ (m), $\varepsilon = 0.02$, and $\delta = 8$, with desired configurations $\mathbf{q}_1^d = [\frac{1}{2}\pi, -\frac{1}{2}\pi, -\frac{1}{2}\pi, \frac{1}{2}\pi]^T$ (rad) and $\mathbf{q}_2^d = [\frac{1}{2}\pi, \frac{1}{2}\pi, \frac{1}{6}\pi, \frac{1}{2}\pi]^T$ (rad).

Table I. *Parameters for the planar manipulators.*

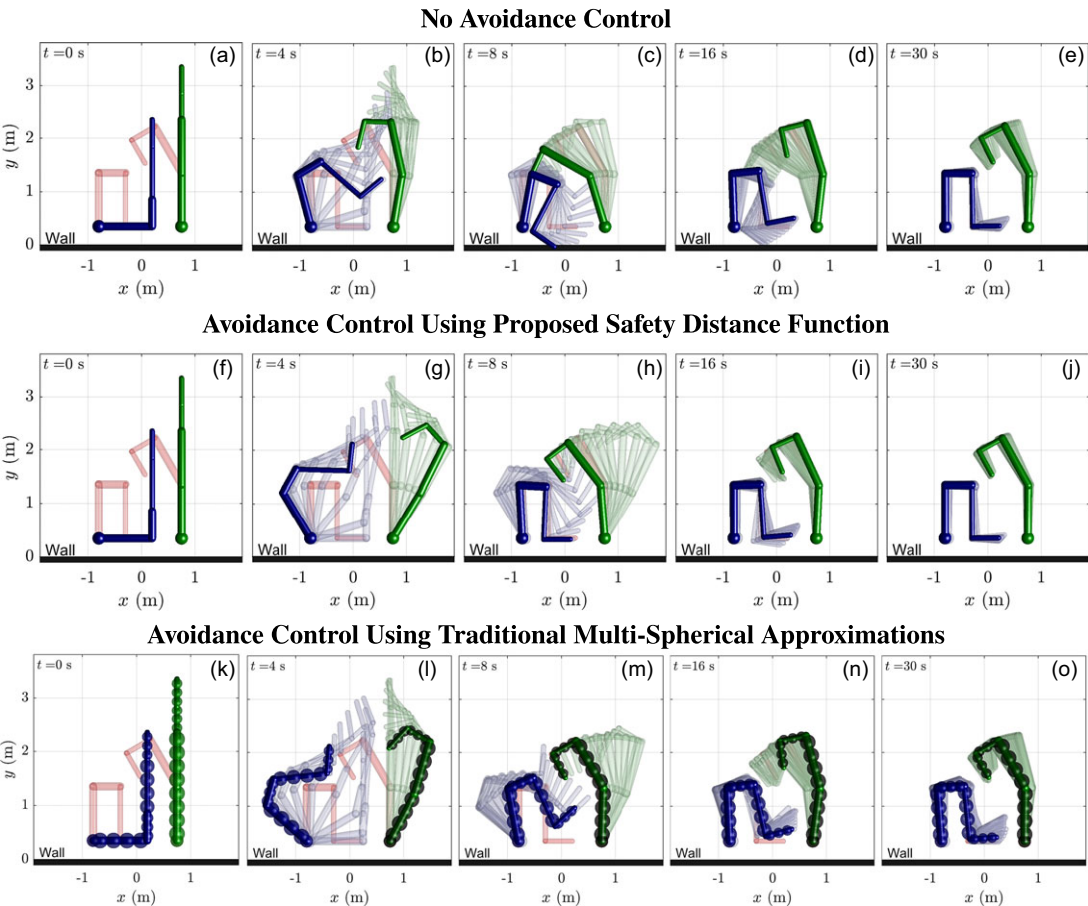| Parameter	Robot 1				Robot 2: Links			
	Link 1	Link 2	Link 3	Link 4	Link 1	Link 2	Link 3	Link 4
ℓ_{ij} (m)	1.0	0.5	1.0	0.5	1.0	1.0	0.5	0.5
w_{ij} (m)	0.15	0.15	0.1	0.1	0.15	0.15	0.1	0.1
m_{ij} (kg)	2.0	1.0	2.0	1.0	2.0	2.0	1.0	1.0
Parameters for Traditional Avoidance Control with Spherical Approx.								
# of Spheres	4	3	4	3	4	4	3	3
radius (m)	0.146	0.112	0.135	0.097	0.146	0.146	0.097	0.097

Figure 3. *Simulation of two 4-DOF planar manipulators interacting with a wall. The top row (a)–(e) Illustrates the case of no avoidance control, the row in the middle (f)–(j) depicts the case of the proposed avoidance control, while the lower row (k)–(o) depicts the use of artificial potential field functions (11) with links approximated by a collection of spheres. The first and second robots are denoted in blue and green, respectively, with the desired configurations given in red. The sequential motion of both manipulators is illustrated by the transparent configurations time spaced by 0.5 (s).*
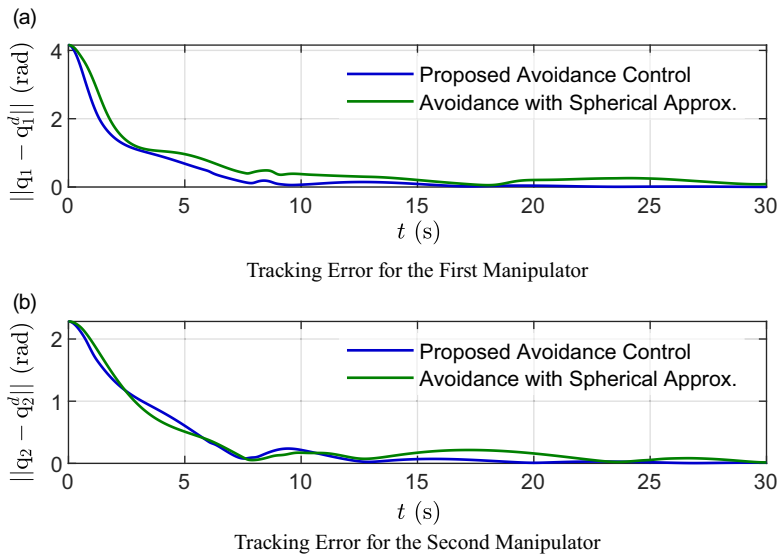
Figure 4. *Vector norm of the configuration errors for both manipulators.*

The results for the case in which no-collision control is applied, that is, $\mathbf{u}_{ij}^{kl} \equiv \mathbf{0}$, are given in Figs. 3(a)-(e). Note that the robots, illustrated in blue and green with desired configurations in red, encounter a collision with each other at $t \approx 8$ (s) (see Fig. 3(c)). The first robot collides with the wall at $t \approx 8$ (s) and with itself moments later (see Fig. 3(d)), before stabilizing at the final desired configuration.
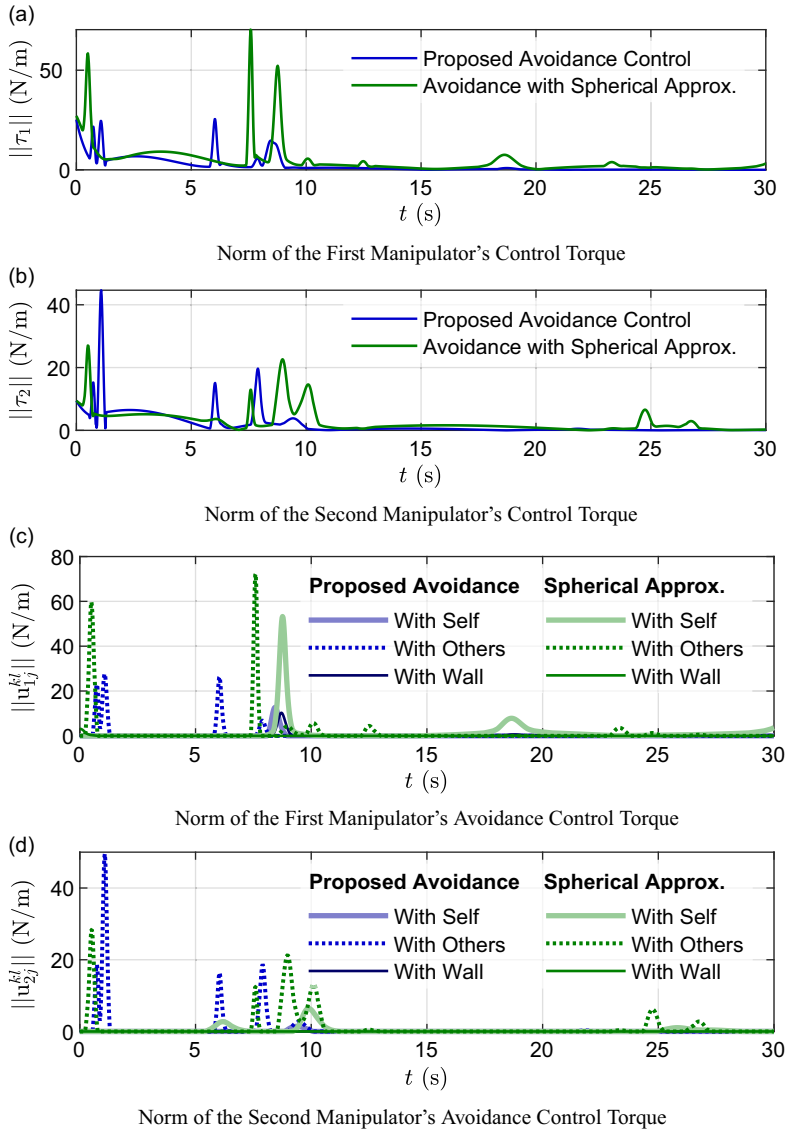
The manipulators are then simulated with the proposed control strategy, with results illustrated in Figs. 3(f)-(j). The static wall is simulated as another rectangular link, centered at $x = y = 0$ (m), with zero orientation, and with length and width equal to 6 (m) and 0.05 (m). Note that the robotic manipulators can successfully converge to the desired configurations while avoiding collisions with each other, with themselves, and with the wall.

For the sake of comparison, Figs. 3(k)–(o) show the sequential motion of the manipulators when the traditional artificial potential functions (11) are applied, and the links are approximated by a collection of spheres centered along the links' axes. The number of spheres per link, as well as their radius, are given in Table I, where the location and radius were chosen such that the links are entirely covered without any overlapping. The manipulators avoid all collisions, but as seen in Figs. 3(n) and 3(o), the manipulators took a longer time to converge to their desired configurations.

Finally, Figs. 4 and 5 depict the norm of the tracking errors and control torques when using the proposed method and the traditional artificial potential field functions with spherical approximations. Note that, in general, the proposed avoidance control had a slightly faster convergence and lower torques. This might be due, in part, to the consideration of more artificial potential field functions when computing the control torques using the traditional approach, which approximates links and obstacles with a collection of spheres. In addition, the proposed continuously differentiable minimum safe distance can provide, in general, a tighter bound on the distance to a collision, reducing the interference of artificial potential field forces.

4.2. Example: 3D manipulators

Consider now a group of $3-$dimensional n_i-DOF manipulators with dynamics given by (5) and link coordinates $\mathbf{p}_{ij} = [x_{ij}, y_{ij}, z_{ij}]^T$ and $\boldsymbol{\theta}_{ij} = [\phi_{ij}, \vartheta_{ij}, \psi_{ij}]^T$. Once again, we assume that the links can be approximated by right circular cylinders with length ℓ_{ij} and diameter w_{ij} and that their lengths are defined along the x-axis. To approximate the minimum distance, we will start by projecting the links into the xy- zx-, and yz-planes as rectangles and approximating the minimum safe distance in each case using (39).

(a)

Norm of the First Manipulator's Control Torque

(b)

Norm of the Second Manipulator's Control Torque

(c)

Norm of the First Manipulator's Avoidance Control Torque

(d)

Norm of the Second Manipulator's Avoidance Control Torque

Figure 5. *Vector norm of the control torques. Figures (c) and (d) depict the avoidance control torques for the first and second manipulators when avoiding self-collisions (thick line), collisions with the other manipulator (dotted line), and collisions with the wall (fine line).*

Define $R_x(a)$, $R_y(b)$, and $R_z(c)$ as the 3×3 orthogonal rotational matrices representing rotations by a, b, and c about the x-, y-, and z-axis, respectively. Define

$$\begin{bmatrix} \hat{x}_{ij} \\ \hat{y}_{ij} \\ \hat{z}_{ij} \end{bmatrix} = R_z(\phi_{ij})R_y(\vartheta_{ij})R_x(\psi_{ij}) \begin{bmatrix} \ell_{ij} \\ 0 \\ 0 \end{bmatrix} \tag{41}$$

which represents the (x, y, z) coordinates of the line $\vec{\ell}_{ij}$ passing through the center of the cylinder after the three rotations, as denoted in Figure 6a. Then, the projected lengths and orientations of the links in
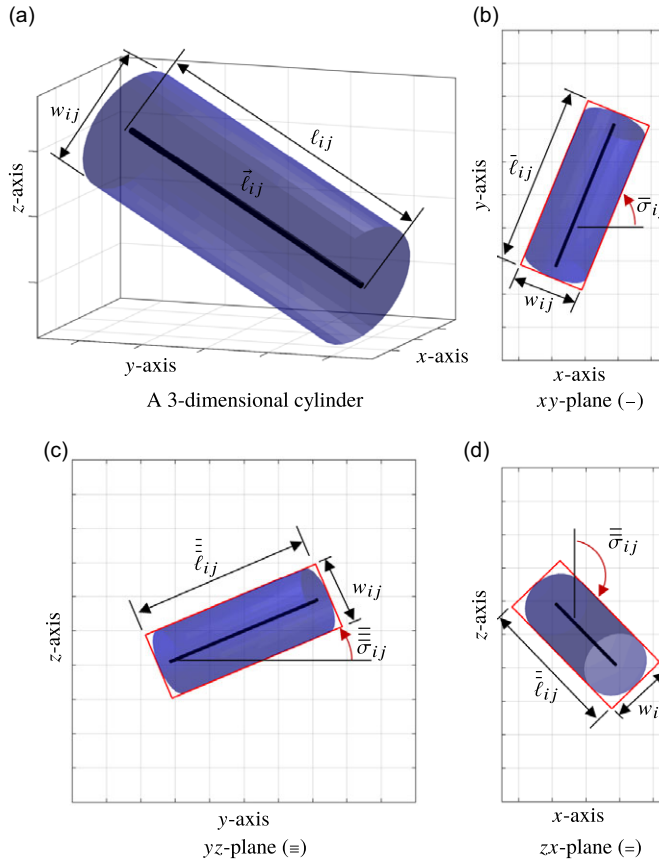
Figure 6. *Planar projections of a 3D cylinder into the xy-, yz-, and zx-planes.*

all three Cartesian planes can be approximated from above by:

$$\bar{\ell}_{ij} = \sqrt{\hat{x}_{ij}^2 + \hat{y}_{ij}^2 + \varepsilon^2} + \frac{w_{ij}\tilde{\alpha}_\varepsilon(\hat{z}_{ij})}{\ell_{ij}}, \qquad \bar{\sigma}_{ij} = \text{atan2}(\hat{y}_{ij}, \hat{x}_{ij}) \tag{42a}$$

$$\bar{\bar{\ell}}_{ij} = \sqrt{\hat{x}_{ij}^2 + \hat{z}_{ij}^2 + \varepsilon^2} + \frac{w_{ij}\tilde{\alpha}_\varepsilon(\hat{y}_{ij})}{\ell_{ij}}, \qquad \bar{\bar{\sigma}}_{ij} = -\text{atan2}(\hat{z}_{ij}, \hat{x}_{ij}) \tag{42b}$$

$$\bar{\bar{\bar{\ell}}}_{ij} = \sqrt{\hat{y}_{ij}^2 + \hat{z}_{ij}^2 + \varepsilon^2} + \frac{w_{ij}\tilde{\alpha}_\varepsilon(\hat{x}_{ij})}{\ell_{ij}}, \qquad \bar{\bar{\bar{\sigma}}}_{ij} = \text{atan2}(\hat{z}_{ij}, \hat{y}_{ij}) \tag{42c}$$

for some small $\varepsilon > 0$, where $(\bar{\ell}_{ij}, \bar{\sigma}_{ij})$, $(\bar{\bar{\ell}}_{ij}, \bar{\bar{\sigma}}_{ij})$, and $(\bar{\bar{\bar{\ell}}}_{ij}, \bar{\bar{\bar{\sigma}}}_{ij})$ denote the lengths and orientations of the links when projected to the xy-, zx-, and yz-planes, respectively. In what follows, we will use the accents $-$, $=$, and $\equiv$ to denote variables in the xy-, yz-, and zx-planes. The addition of ε and $\tilde{\alpha}_\varepsilon(\cdot)$ in the approximations is to guarantee that the projected lengths are continuous differentiable functions. The width of the rectangular shapes, on the other hand, is always equal to the diameter of the cylinder, w_{ij}. Fig. 6 illustrates an example of the equivalent rectangular shapes projected in each plane.

Once the dimensions and orientations of each pair of links in each Cartesian plane is defined, one can approximate the minimum safe distance between two projected links in xy-, zx-, and yz-plane as:

$$\bar{r}_{ij}^{kl} = \tilde{\lambda}_\delta(\bar{\varrho}_{ij}^{kl}, \bar{\varrho}_{kl}^{ij}), \qquad \bar{\bar{r}}_{ij}^{kl} = \tilde{\lambda}_\delta(\bar{\bar{\varrho}}_{ij}^{kl}, \bar{\bar{\varrho}}_{kl}^{ij}), \qquad \bar{\bar{\bar{r}}}_{ij}^{kl} = \tilde{\lambda}_\delta(\bar{\bar{\bar{\varrho}}}_{ij}^{kl}, \bar{\bar{\bar{\varrho}}}_{kl}^{ij}) \tag{43}$$

Table II.   *Parameters for the 3D manipulators.*

Parameter	Link 1	Link 2	Link 2	Link 4	Link 5
ℓ_{ij} (m)	0.45	0.3	0.3	0.4	0.4
w_{ij} (m)	0.08	0.05	0.05	0.04	0.04
m_{ij} (kg)	2.0	1.5	1.5	1.0	1.0
Parameters for Traditional Avoidance Control with Spherical Approx.					
# of Spheres	7	5	5	6	6
radius (m)	0.051	0.039	0.039	0.039	0.039

for some large $\delta > 0$, where $\tilde{\lambda}_\delta(\cdot)$ is the minimum approximation function from above and

$$\underline{\varrho}_\star^\dagger := \varrho(\underline{\ell}_\star, \underline{\ell}_\dagger, w_\star, w_\dagger, \overline{\sigma}_\star, \overline{\sigma}_\dagger, \overline{\varphi}_\star^\dagger), \qquad \overline{\varphi}_\star^\dagger := \operatorname{atan2}(y_\dagger - y_\star, x_\dagger - x_\star) - \overline{\sigma}_\star \qquad (44a)$$

$$\overline{\overline{\varrho}}_\star^\dagger := \varrho(\overline{\overline{\ell}}_\star, \overline{\overline{\ell}}_\dagger, w_\star, w_\dagger, \overline{\overline{\sigma}}_\star, \overline{\overline{\sigma}}_\dagger, \overline{\overline{\varphi}}_\star^\dagger), \qquad \overline{\overline{\varphi}}_\star^\dagger := \operatorname{atan2}(x_\dagger - x_\star, z_\dagger - z_\star) - \overline{\overline{\sigma}}_\star \qquad (44b)$$

$$\overline{\overline{\overline{\varrho}}}_\star^\dagger := \varrho(\overline{\overline{\overline{\ell}}}_\star, \overline{\overline{\overline{\ell}}}_\dagger, w_\star, w_\dagger, \overline{\overline{\overline{\sigma}}}_\star, \overline{\overline{\overline{\sigma}}}_\dagger, \overline{\overline{\overline{\varphi}}}_\star^\dagger), \qquad \overline{\overline{\overline{\varphi}}}_\star^\dagger := \operatorname{atan2}(z_\dagger - z_\star, y_\dagger - y_\star) - \overline{\overline{\overline{\sigma}}}_\star \qquad (44c)$$

for $\{\star, \dagger\} \in \{ij, kl\}$. Now, let's define the minimum safe distance (in 3D) between the centers of ijth and klth links along the vector $\mathbf{p}_{ij} - \mathbf{p}_{kl}$ as:

$$r_{ij}^{kl} = r_{kl}^{ij} = h \left\| \mathbf{p}_{ij} - \mathbf{p}_{kl} \right\| \qquad (45)$$

where $h > 0$. To ensure that the links do not collide, one needs to guarantee that at least one of the Cartesian plane's minimum safe distance is satisfied. Mathematically, this means that one of the following inequalities holds

$$h \cdot \left((x_{ij} - x_{kl})^2 + (y_{ij} - y_{kl})^2 \right) \geq (\overline{r}_{ij}^{kl})^2 \qquad (46a)$$

$$h \cdot \left((x_{ij} - x_{kl})^2 + (z_{ij} - z_{kl})^2 \right) \geq (\overline{\overline{r}}_{ij}^{kl})^2 \qquad (46b)$$

$$h \cdot \left((y_{ij} - y_{kl})^2 + (z_{ij} - z_{kl})^2 \right) \geq (\overline{\overline{\overline{r}}}_{ij}^{kl})^2. \qquad (46c)$$

Accordingly, one can pick h as:

$$h = \left(\tilde{\Lambda}_\delta \left(\frac{(x_{ij} - x_{kl})^2 + (y_{ij} - y_{kl})^2}{(\overline{r}_{ij}^{kl})^2}, \frac{(x_{ij} - x_{kl})^2 + (z_{ij} - z_{kl})^2}{(\overline{\overline{r}}_{ij}^{kl})^2}, \frac{(y_{ij} - y_{kl})^2 + (z_{ij} - z_{kl})^2}{(\overline{\overline{\overline{r}}}_{ij}^{kl})^2} \right) \right)^{-1} \qquad (47)$$

where $\tilde{\Lambda}_\delta(\cdot)$ is the smooth approximation of the maximum function from above (9). Note that $\overline{r}_{ij}^{kl}$, $\overline{\overline{r}}_{ij}^{kl}$, and $\overline{\overline{\overline{r}}}_{ij}^{kl}$ are by definition larger than the cross-sectional radius of the links, that is, larger than $(w_{ij} + w_{kl})/2 > 0$, and therefore, h and r_{ij}^{kl} are well defined and continuously differentiable.

An example with two identical 5-DOF revolute robotic manipulators is now presented. The system parameters for the robots are given in Table II. The robots are assumed to be tasked with lifting an object centered at $(x, y, z) = (0.5, 0, -0.3)$ (m). Accordingly, the desired configurations are chosen as $\mathbf{q}_1^d = [1.13, -2.23, 2.59, 1.44, 3.01]^T$ (rad) and $\mathbf{q}_2^d = [0.32, -2.23, 2.59, 1.44, 3.01]^T$ (rad). The robots must also avoid a wall located at $x = -0.15$ (m).

The simulation results with the proposed avoidance control are given in Fig. 7. The control parameters are chosen as $A_i = \operatorname{diag}(15, 15, 12, 12, 12)$, $B_i = \operatorname{diag}(8, 8, 8, 8, 8)$, $\rho_{ij}^{kl} = 0.25$ (m), $\varepsilon = 0.02$, and $\delta = 8$. As can be observed from the snapshots, both manipulators stayed away from collisions and converged to the desired configuration in less than 15 s.

We also simulated the robotic manipulators using spherical approximations and applying the traditional artificial potential field approach (11) with a constant radius. Given the fact that the spherical approximation augments the size of the links, a slightly smaller safety range of $\rho_{ij}^{kl} = 0.2$ (m) was chosen to ease mobility. The results are shown in Fig. 8. Note that the robots avoided collisions but took longer to converge. In fact, after 15 (s), the robots have not quite stabilized yet at the desired position.
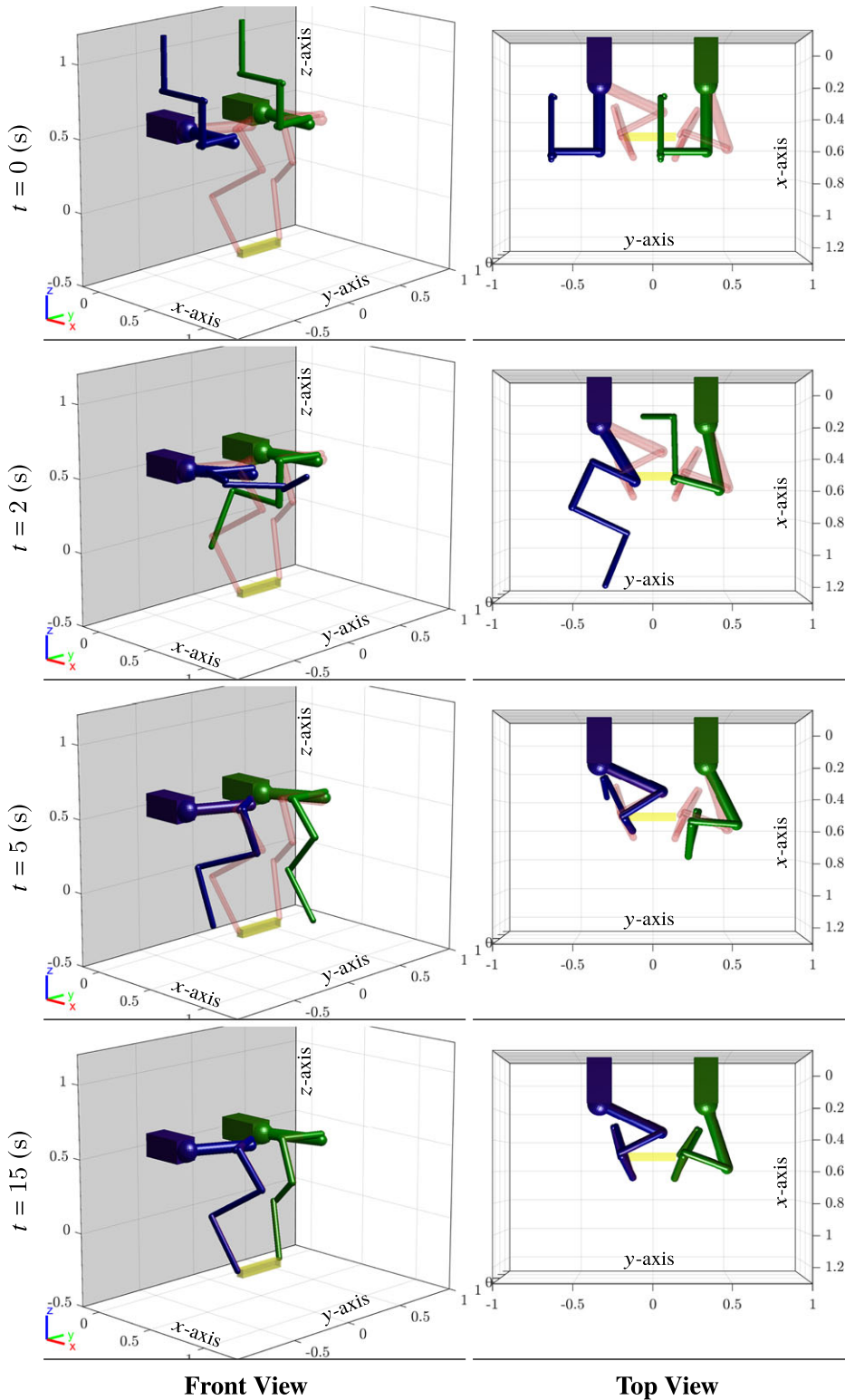
Figure 7. *Simulation of two identical three-dimensional robots with proposed avoidance control. The desired configurations are illustrated in red, with the simulated object to be picked up in yellow.*
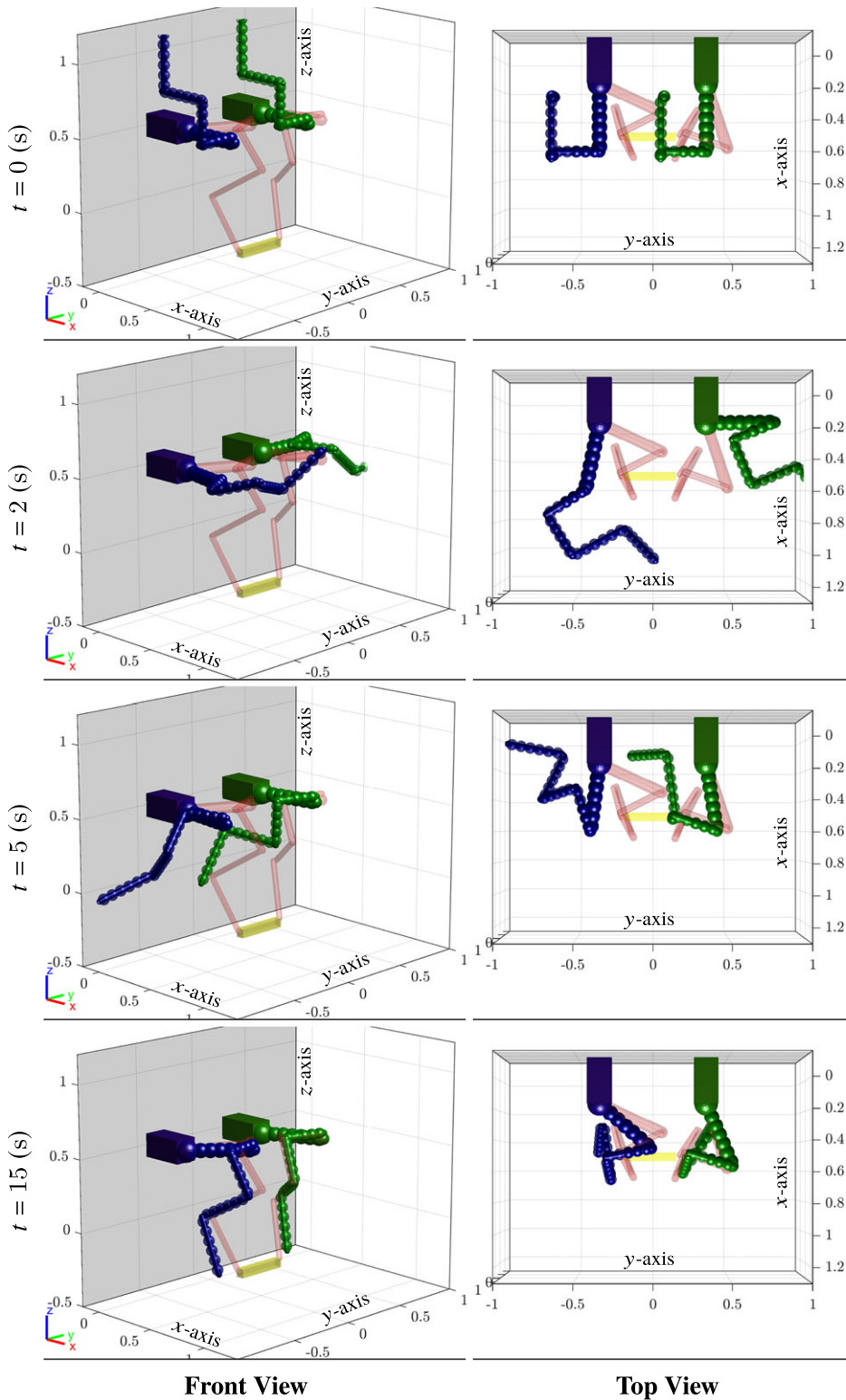
Figure 8. *Simulation of two identical three-dimensional robots using spherical approximations for the links and the wall. The desired configurations are illustrated in red, with the simulated object to be picked up in yellow.*
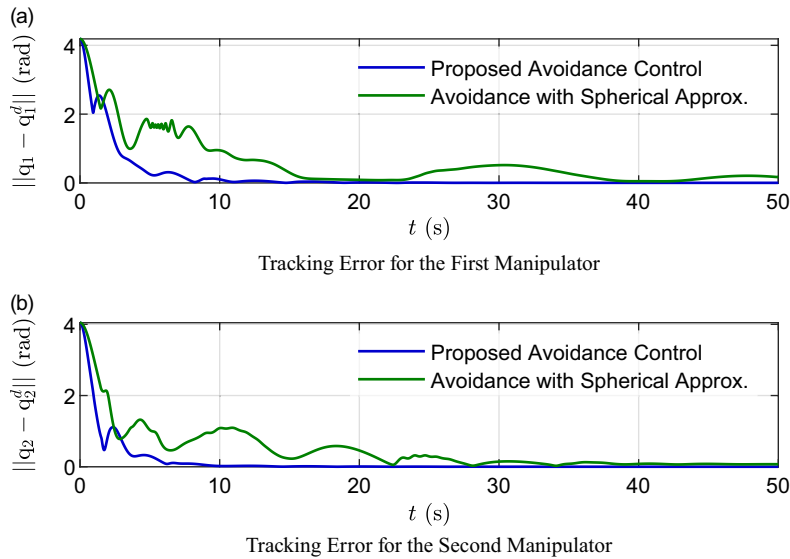
Figure 9. *Vector norm of the configuration errors for both 5-DOF manipulators.*

For comparison, Figs. 9 and 10 illustrate the norm of tracking error in generalized coordinates and the control torques for both manipulators, respectively. Note that while the manipulators under the proposed avoidance control converged to the desired configuration in approximately 10 (s), it took more than 50 (s) for both manipulators to converge under the traditional use of spherical approximations. This can be attributed to the interference with the desired task by several repulsive field forces generated by multiple spheres. In addition, the proposed continuously differentiable minimum safe distance may provide a tighter distance to collision bound than the approximation of elongated obstacles with spheres, increasing the maneuverability of links through obstructed spaces. Finally, the control torques under the traditional approach are also significantly higher than with the proposed avoidance control. The latter can also be attributed to the interaction of multiple repulsive potential field functions. It is worth noting that the spikes in the magnitude of the control torques are due to the repulsive forces, which tend to rapidly increase when the distance between the link and the obstacle approaches zero.

4.3. Example: 3D manipulators with bounded torques

Next, we consider the case of robotic manipulators with bounded control torques.

Consider the two-robot system from Section 4.2 with parameters given in Table II. Assume now that the control torque for each link is bounded by $T_{i1} = T_{i2} = 100$ (Nm), $T_{i3} = 80$ (Nm), and $T_{i4} = T_{i5} = 60$ (Nm) for $i \in \{1, 2\}$ and that the system implements the saturated PD-type control with gravity compensation and collision avoidance strategy from Section 3.3.6, equation (28). Let the control parameters for the minimum safety distance and PD control be the same as in Section 4.2 but with saturation bounds for the PD control given by $\omega_{ij} = \frac{1}{2}T_{ij} \forall i, j$. Similarly, let the bounds on the gravitational torques be $G_{i1} = G_{i2} = 0$ (Nm), $G_{i3} = 30$ (Nm), $G_{i4} = 16$ (Nm), and $G_{i5} = 6$ (Nm), which have been obtained by numerical estimation. Finally, since the avoidance control term in (28) can exceed the manipulators' input control bounds, the total input torque τ_{ij} is further saturated at $-T_{ij}$ and T_{ij} whenever it exceeds these bounds.

The simulation results under the saturated PD-type control with gravity compensation and collision avoidance strategy are illustrated in Fig. 11. Note that both manipulators are able to converge safely to the desired configurations within 15 (s), similar to the use of the unbounded control law as presented in Section 4.2. Fig. 12 compares the implementation of both controllers in terms of tracking error. Observe
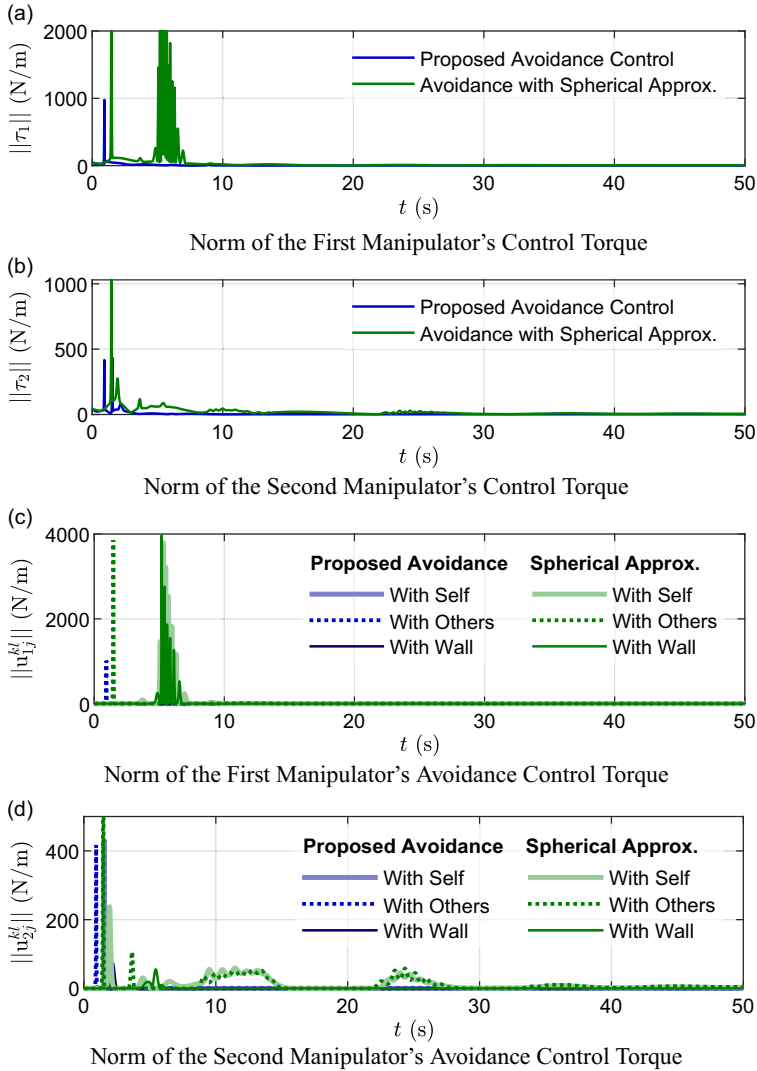
Figure 10. *Vector norm of the control torques for both 5-DOF manipulators. Figures (c) and (d) depict the avoidance control torques for the first and second manipulators when avoiding self-collisions (thick line), collisions with the other manipulator (dotted line), and collisions with the wall (fine line).*

that the responses of the unsaturated control (16) and the saturated one (28) exhibit similar behaviors, with the saturated PD-type control taking just slightly longer to converge.

Fig. 13 shows the magnitude of the total control torque (i.e., $|\tau_{ij}|$), the saturated PD-type control (i.e., $|\text{sat}_{ij}(a_{ij}\tilde{q}_{ij} + b_{ij}\dot{q}_{ij})|$), the gravitational torque (i.e., $|g_{ij}|$), and the total collision avoidance control torque (i.e., $|\bar{u}_{ij}|$) for each manipulator's joint. Note that the total control torque remains within its bound T_{ij} at all times, reaching the maximum only when the avoidance control is also large. These maximum, rapidly increasing control torque values result from the repulsive forces when a link rapidly approaches an obstacle and are to be expected among potential field-based methods. Note that the saturated PD-type control torque remains within its bound ω_{ij}, and the sum of the gravitational compensation torque and the PD-type control never exceeds the total control bound. The avoidance control also remains within the required bound $U_{ij} = T_{ij} - G_{ij} - \omega_{ij}$ for guaranteed collision avoidance most of the time except at
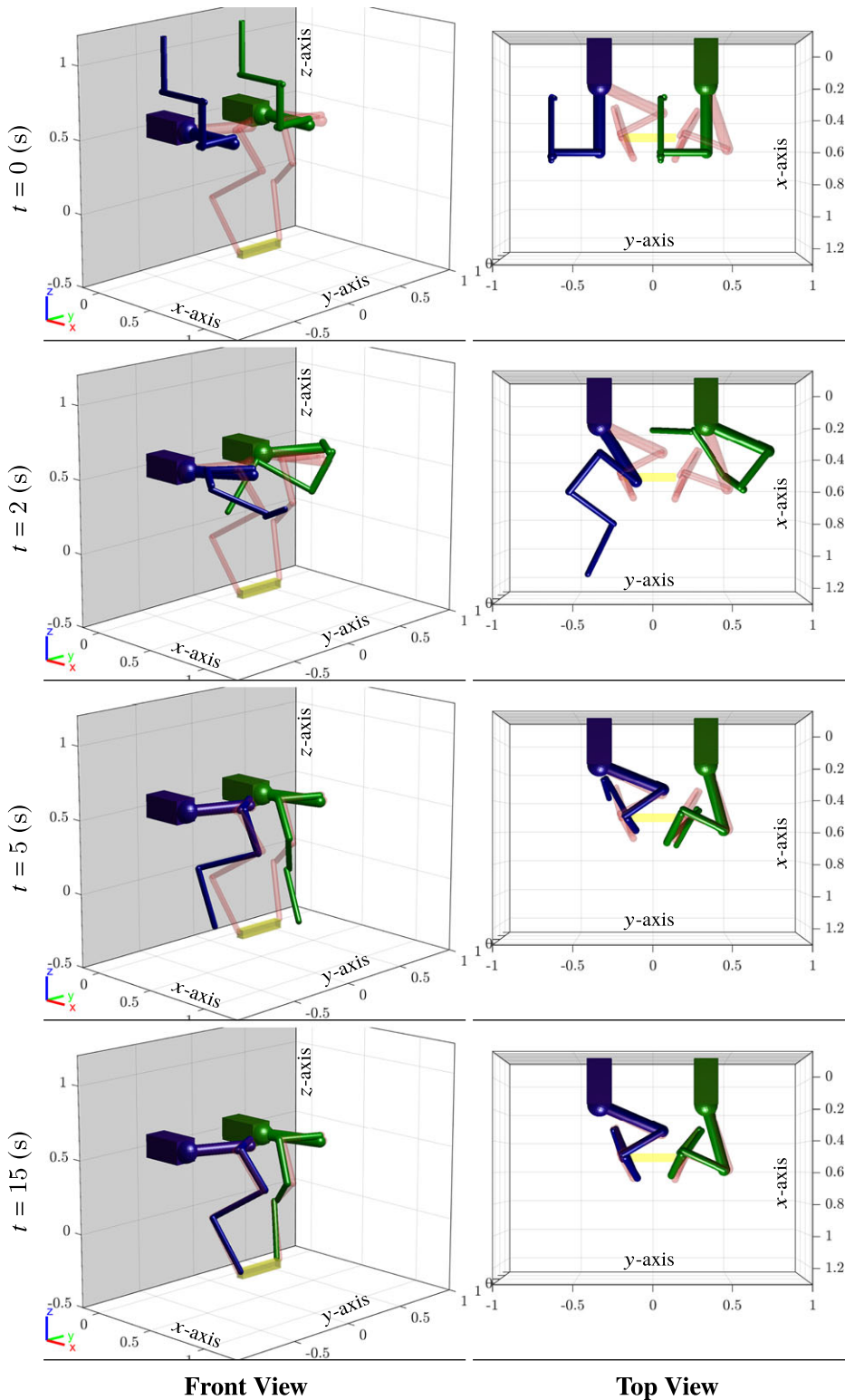
Figure 11. *Simulation of two identical three-dimensional robots with bounded control torques and proposed avoidance control. The desired configurations are illustrated in red, with the simulated object to be picked up in yellow.*
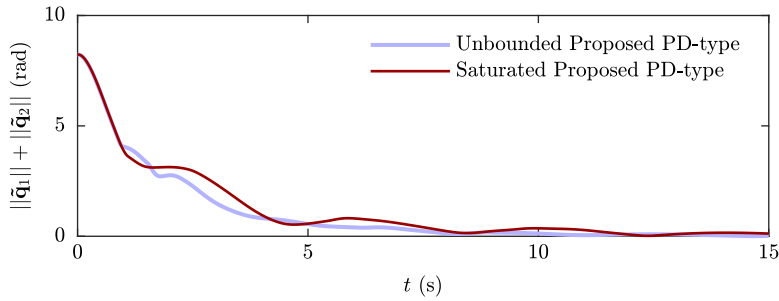
Figure 12. *Comparison of the norm of the tracking error, $\|\tilde{q}_1\| + \|\tilde{q}_2\|$, when using the unbounded PD-type control ([16a](#)) and the saturated PD-type control ([28](#)).*
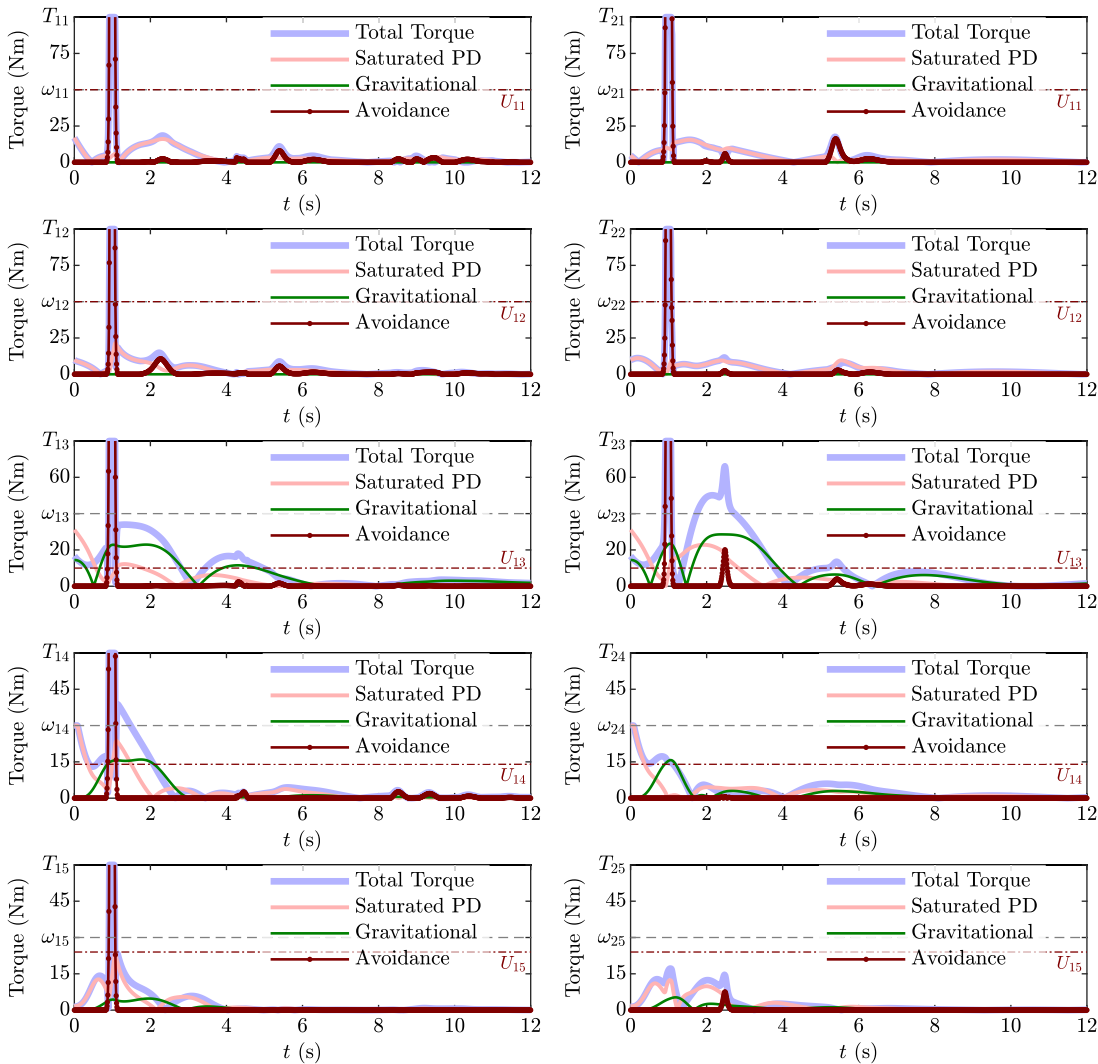
Figure 13. *Norm of links' control torques for the first robot (left-side) and second robot (right-side).*

critically safety instances when the links come close to a collision. Nevertheless, both manipulators are able to avoid collisions at all times.

5. Conclusions and Future Work

This paper presented a cooperative, distributed avoidance control law for multiple robotic manipulators. The control strategy builds on the concepts of potential field functions and approximates the links and obstacles as shapes of smooth radii. However, in contrast to previous work, the proposed avoidance control law reduces the conservatism of other potential field methods by avoiding the traditional spherical and elliptical shape assumptions. Similarly, the control input torques are smooth, well-defined, closed-form functions, simplifying the implementation and avoiding the discontinuities of other shortest distance-based methods. Furthermore, the control approach is also rigorously shown to prevent collisions at all times using Lyapunov analysis. Extensions to robotic manipulators with bounded control torques and other Lyapunov-based tracking controllers are also given. Simulation examples with 2D and 3D revolute manipulators demonstrate the performance of the avoidance control strategy in comparison to traditional spherical approximations.

Author contributions. E. Rodriguez-Seda conceived the general idea, designed the control framework, developed the theory, conducted the simulations and analysis, and prepared the first draft of the manuscript. M. Kutzer contributed to the motivation and conception of the control problem, provided critical expertise on robotic manipulator dynamics and simulation, and revised the manuscript.

Competing interests. The authors declare no conflicts of interest exist.

Ethical approval. None.

References

[1] H. Christensen, N. Amato, H. Yanco, M. Mataric, H. Choset, A. Drobnis, K. Goldberg, J. Grizzle, G. Hager, J. Hollerbach, S. Hutchinson, V. Krovi, D. Lee, W. D. Smart, J. Trinkle and G. Sukhatme, "A roadmap for US robotics–From internet to robotics 2020 edition," *Found Trend Robot* **8**(4), 307–424 (2021).

[2] G. Palmieri and C. Scoccia, "Motion planning and control of redundant manipulators for dynamical obstacle avoidance," *Machines* **9**(6), 121 (2021).

[3] T. Lozano-Pérez, *Spatial Planning: A Configuration Space Approach* (Springer, New York, NY, 1990) pp. 259–271.

[4] S. Karaman and E. Frazzoli, "Optimal Kinodynamic Motion Planning using Incremental Sampling-Based Methods," **In:** *IEEE Conference on Decision and Control*, (2010) pp. 7681–7687.

[5] S. M. LaValle, J. J. Kuffner and B. Donald, "Rapidly-Exploring Random Trees: Progress and Prospects," **In:** *Algorithmic and Computational Robotics: New Directions*, B. Donald, K. Lynch and D. Rus (2001) pp. 293–308.

[6] T. Rybus, J. Prokopczuk, M. Wojtunik, K. Aleksiejuk and J. Musiał, "Application of bidirectional rapidly exploring random trees (BiRRT) algorithm for collision-free trajectory planning of free-floating space manipulator," *Robotica* **40**(12), 4326–4357 (2022).

[7] D. Hsu, R. Kindel, J.-C. Latombe and S. Rock, "Randomized kinodynamic motion planning with moving obstacles," *Int J Robot Res* **21**(3), 233–255 (2002).

[8] G. B. Avanzini, A. M. Zanchettin and P. Rocco, "Constrained model predictive control for mobile robotic manipulators," *Robotica* **36**(1), 19–38 (2018).

[9] P. Xu, N. Wang, S.-L. Dai and L. Zuo, "Motion planning for mobile robot with modified bit∗ and mpc," *Appl Sci* **11**(1), 426 (2021).

[10] X. Tang, H. Zhou and T. Xu, "Obstacle avoidance path planning of 6-dof robotic arm based on improved A* algorithm and artificial potential field method," *Robotica* **42**(2), 457–481 (2024).

[11] D. Yang, L. Dong and J. K. Dai, "Collision avoidance trajectory planning for a dual-robot system: Using a modified APF method," *Robotica* **42**(3), 846–863 (2024).

[12] S. Agarwal, R. A. Srivatsan and S. Bandyopadhyay, "Analytical determination of the proximity of two right-circular cylinders in space," *J Mech Robot* **8**(4), 041010 (2016).

[13] S. Moe, K. Y. Pettersen and J. T. Gravdahl, "Set-based collision avoidance applications to robotic systems," *Mechatronics* **69**, 102399 (2020).

[14] R. V. Patel, F. Shadpey, F. Ranjbaran and J. Angeles, "A collision-avoidance scheme for redundant manipulators: Theory and experiments," *J Robot Syst* **22**(12), 737–757 (2005).

[15] D. Rakita, B. Mutlu and M. Gleicher, "Proxima: An Approach for Time or Accuracy Budgeted Collision Proximity Queries," **In:** *Proceedings of Robotics: Science and Systems* (2022) pp. 1–13.

[16] J. Schulman, Y. Duan, J. Ho, A. Lee, I. Awwal, H. Bradlow, J. Pan, S. Patil, K. Goldberg and P. Abbeel, "Motion planning with sequential convex optimization and convex collision checking," *Int J Robot Res* **33**(9), 1251–1270 (2014).

[17] B. Sangiovanni, G. P. Incremona, M. Piastra and A. Ferrara, "Self-configuring robot path planning with obstacle avoidance via deep reinforcement learning," *IEEE Control Syst Lett* **5**(2), 397–402 (2020).

[18] T. Zhang, K. Zhang, J. Lin, W.-Y. G. Louie and H. Huang, "Sim2real learning of obstacle avoidance for robotic manipulators in uncertain environments," *IEEE Robot Autom Lett* **7**(1), 65–72 (2021).

[19] L. Zlajpah and B. Nemec, "Kinematic Control Algorithms for On-Line Obstacle Avoidance for Redundant Manipulators," **In:** *IEEE/RSJ International Conference on Intelligent Robots and Systems*, (2002) pp. 1898–1903.

[20] O. Khatib, "Real-time obstacle avoidance for manipulators and mobile robots," *Int J Robot Res* **5**(1), 90–98 (1986).

[21] G. Leitmann and J. Skowronski, "Avoidance control," *J Optim Theory Appl* **23**(4), 581–591 (1977).

[22] S. A. Deka, X. Li, D. M. Stipanović and T. Kesavadas, "Robust and safe coordination of multiple robotic manipulators: An approach using modified avoidance functions," *J Intell Robot Syst* **90**(3-4), 419–435 (2018).

[23] E. J. Rodríguez-Seda and D. M. Stipanović, "Cooperative avoidance control with velocity-based detection regions," *IEEE Control Syst Lett* **4**(2), 432–437 (2020).

[24] R. Volpe and P. Khosla, "Manipulator control with superquadric artificial potential functions: Theory and experiments," *IEEE Trans Syst Man Cybern* **20**(6), 1423–1436 (1990).

[25] W. Wang, M. Zhu, X. Wang, S. He, J. He and Z. Xu, "An improved artificial potential field method of trajectory planning and obstacle avoidance for redundant manipulators," *Int J Adv Robot Syst* **15**(5), 1–13 (2018).

[26] H. Xie, R. V. Patel, S. Kalaycioglu and H. Asmer, "Real-time Collision Avoidance for a Redundant Manipulator in an Unstructured Environment," **In:** *IEEE/RSJ International Conference on Intelligent Robots and Systems*, (1998) pp. 1925–1930.

[27] T. Zhu, J. Mao, L. Han, C. Zhang and J. Yang, "Real-time dynamic obstacle avoidance for robot manipulators based on cascaded nonlinear mpc with artificial potential field," *IEEE Trans Ind Electron* **71**(7), 7424–7434 (2024).in press.

[28] W. Zhang, E. J. Rodríguez-Seda, S. A. Deka, M. Amrouche, D. Zhou, D. M. Stipanović and G. Leitmann, "Avoidance control with relative velocity information for lagrangian dynamics," *J Intell Robot Syst* **99**(2), 229–244 (2020).

[29] S. Stavridis, D. Papageorgiou and Z. Doulgeri, "Dynamical system based robotic motion generation with obstacle avoidance," *IEEE Robot Autom Lett* **2**(2), 712–718 (2017).

[30] S. Zimmermann, M. Busenhart, S. Huber, R. Poranne and S. Coros, "Differentiable Collision Avoidance Using Collision Primitives," **In:** *IEEE/RSJ International Conference on Intelligent Robots and Systems*, (2022) pp.8086–8093.

[31] A. D. Ames, S. Coogan, M. Egerstedt, G. Notomista, K. Sreenath and P. Tabuada, "Control Barrier Functions: Theory and Applications," **In:** *European Control Conference*, (2019) pp.3420–3431.

[32] A. Singletary, K. Klingebiel, J. Bourne, A. Browning, P. Tokumaru and A. Ames, "Comparative Analysis of Control Barrier Functions and Artificial Potential fields for Obstacle Avoidance," **In:** *IEEE/RSJ International Conference on Intelligent Robots and Systems*, (2021) pp. 8129–8136.

[33] A. Singletary, S. Kolathaya and A. D. Ames, "Safety-critical kinematic control of robotic systems," *IEEE Control Syst Lett* **6b**, 139–144 (2022b).

[34] A. Singletary, W. Guffey, T. G. Molnar, R. Sinnet and A. D. Ames, "Safety-critical manipulation for collision-free food preparation," *IEEE Robot Autom Lett* **7a**(4), 10954–10961 (2022a).

[35] S. S. M. Salehian, N. Figueroa and A. Billard, "A unified framework for coordinated multi-arm motion planning," *Int J Robot Res* **37**(10), 1205–1232 (2018).

[36] N. Ratliff, M. Zucker, J. A. Bagnell and S. Srinivasa, "CHOMP: Gradient Optimization Techniques for Efficient Motion Planning," **In:** *IEEE International Conference on Robotics and Automation*, (2009). pp. 489–494.

[37] M. Koptev, N. Figueroa and A. Billard, "Neural joint space implicit signed distance functions for reactive robot manipulator control," *IEEE Robot Autom Lett* **8**(2), 480–487 (2023).

[38] D. M. Stipanović, P. F. Hokayem, M. W. Spong and D. Šiljak, "Cooperative avoidance control for multiagent systems," *J Dyn Syst Meas Control* **129**(5), 699–707 (2007).

[39] P. J. From, I. Schjølberg, J. T. Gravdahl, K. Y. Pettersen and T. I. Fossen, "On the Boundedness and Skew-Symmetric Properties of the Inertia and Coriolis Matrices for Vehicle-Manipulator Systems," **In:** *Proc. IFAC Symp. Intell. Autonomous Vehicles 2010*, Leece, Italy (2010).

[40] D. M. Stipanović, C. J. Tomlin and G. Leitmann, "Monotone approximations of minimum and maximum functions and multi-objective problems," *Appl Math Optim* **66**(3), 455–473 (2012).

[41] S. Mastellone, D. M. Stipanović, C. R. Graunke, K. A. Intlekofer and M. W. Spong, "Formation control and collision avoidance for multi-agent non-holonomic systems: Theory and experiments," *Int J Robot Res* **27**(1), 107–126 (2008).

[42] M. W. Spong, S. Hutchinson and M. Vidyasagar, *Robot Modeling and Control* (John Wiley & Sons, New York, 2005).

[43] J. Wu, J. Wang and Z. You, "An overview of dynamic parameter identification of robots," *Robot Com Int Manuf* **26**(5), 414–419 (2010).

[44] E. J. Rodríguez-Seda, D. M. Stipanović and M. W. Spong, "Guaranteed collision avoidance for autonomous systems with acceleration constraints and sensing uncertainties," *J Optim Theory Appl* **168**(3), 1014–1038 (2016).

[45] D. M. Stipanović, A. Melikyan and N. Hovakimyan, "Guaranteed strategies for nonlinear multi-player pursuit-evasion games," *Int Game Theory Rev* **12**(1), 1–17 (2010).

[46] D. J. López-Araujo, A. Zavala-Río, V. Santibáñez and F. Reyes, "A generalized scheme for the global adaptive regulation of robot manipulators with bounded inputs," *Robotica* **31**(7), 1103–1117 (2013).

[47] A. Zavala-Río and V. Santibáñez, "Simple extensions of the PD-with-gravity-compensation control law for robot manipulators with bounded inputs," *IEEE Trans Contr Syst Technol* **14**(5), 958–965 (2006).

[48] E. J. Rodríguez-Seda and J. J. Dawkins, "Decentralized cooperative collision avoidance control for unmanned rotorcraft with bounded acceleration," *J Guid Control Dyn* **41**(11), 2445–2454 (2018).